# Image Cover Sheet

| CLASSIFICATION | SYSTEM NUMBER |
|---|---|
| UNCLASSIFIED | 155548 |

**TITLE**

EVALUATION OF ROTMAN LENSES FOR SPACE-BASED RADAR

**System Number:**

**Patron Number:**

**Requester:**

**Notes:**

**DSIS Use only:**

**Deliver to:** FF

National Defence / Défense nationale

# EVALUATION OF ROTMAN LENSES FOR SPACE-BASED RADAR

by

J.W. Moffat

DEFENCE RESEARCH ESTABLISHMENT OTTAWA
REPORT NO. 1271

Canada

December 1995
Ottawa

National Defence / Défense nationale

# EVALUATION OF ROTMAN LENSES FOR SPACE-BASED RADAR

by

**J.W. Moffat**
*MIL SAT Communications Group*
*Space Systems and Technology Section*

**DEFENCE RESEARCH ESTABLISHMENT OTTAWA**
REPORT NO. 1271

PCN
041BD

December 1995
Ottawa

## ABSTRACT

The Space-Based Radar (SBR) R&D Project at DREO has been investigating the feasibility of the application of a number of different technologies to space-based wide area surveillance using microwave radar. One of the technologies investigated was the Rotman lens implementation of a Fourier transform beam forming network. A number of Rotman lenses were designed and manufactured in stripline microwave structure under a development contract. The expected performance was not achieved. A study was initiated to investigate possible causes of this performance deficiency.

This study was divided into two main thrusts. First the lenses were assessed physically using ultrasonic and X-ray technologies, with a confirmation of the results by the sectioning and subsequent microscopic examination of one of the lenses. Following that, some simple stripline structures were measured in a microwave lab in order to gain an understanding of the difficulties of measuring the permittivity of the dielectric material within the structure. This report describes the experiments performed and the results obtained.



## RÉSUMÉ

Le projet R et D de radar spatial à DREO a étudié la possibilité d'appliquer différentes technologies pour la surveillance spatiale de vastes régions au moyen d'un radar à hyperfréquence. Une des technologies étudiées fut l'implémentation par lentilles Rotman d'un réseau de mise en forme de faisceaux par transformée de Fourrier. Un certain nombre de lentilles Rotman ont été développées sous contrat et fabriquées sur des circuits hyperfréquences à structures stripline. La performance prévue n'a pas été atteinte. Une étude a été lancée afin de rechercher les causes possibles de ce manque de performance.

Cette étude fut divisée en deux volets principaux. En premier, les lentilles furent évaluées physiquement au moyen de technologies à ultra-son et à rayons X. Une confirmation des résultats fut obtenu en effectuant un sectionnement d'une des lentilles, suivi d'un examen microscopique. Après celà, quelques structures à lignes microruban simples furent mesurées dans un laboratoire à hyperfréquence afin de mieux comprendre les difficultées associées à la mesure de la perméativité du matériel diélectrique de la structure. Ce rapport décrit les expériences qui ont été faites et les résultats obtenus.

## EXECUTIVE SUMMARY

The Space-Based Radar (SBR) R&D Project at DREO has been investigating the feasibility of the application of a number of different technologies to space-based wide area surveillance using microwave radar. One of the technologies investigated was the Rotman lens implementation of a Fourier transform beam forming network. A number of Rotman lenses were designed and manufactured in stripline microwave structure under a development contract. The expected performance was not achieved. A study was initiated to investigate possible causes of this performance deficiency.

This study focussed initially on manufacturing problems and physical anomalies. The physical structure of the lens was investigated using ultrasonic scanning and X-ray technologies. Some irregularities were found, including possible air gaps between the different layers of the lenses. In order to confirm these results, one of the lenses was selected for microscopic examination. A cut was made through a number of suspect areas, and the exposed surfaces were polished and examined under a microscope. Results of this examination confirmed the presence of delaminations and disbond within the structure, and the presence of substantial air voids.

To lay a foundation for this study, the basics of the operation of the Rotman lens are described. The lens is physically described as two dielectric layers sandwiched between two conducting plates with a printed copper conductor between them. Signals are coupled into and out of the lens through ports around the periphery. The ports are divided into beam ports and antenna ports. Each antenna port is connected to an antenna of a phased array through an appropriate length of cable. Each beam port represents a radiated beam in a discrete direction. The desired direction of the antenna radiation pattern is selected through selection of the port associated with that direction. Any number of beams can be selected simultaneously.

The history of the contracted activity in antenna feed systems and technologies in support of the SBR Project is detailed, along with a description of the Rotman lenses produced under the contracts. Five lenses were produced; four small ones measuring 17 1/2 x 13 1/8 x 9/16", and one large one measuring 48 1/4 x 33 1/2 x 9/16". Two of the small lenses and the large lens were made by the splicing together of four sheets of dielectric for each layer of the lens.

The physical inspection of the lenses began with an ultrasonic examination of the lenses. The basic principles of ultrasonic scanning are described. The device under test is placed into a water bath and a transmitting transducer is passed over it. The receiving sensor measures the reflected energy from the defects within the medium, and they are displayed on a planar view of the lens. The ultrasonic scans of

the lenses showed the primary features of the lenses. These included lens outline, port locations, copper foil outline with stepped impedance matching transformers, the presence and location of the dielectric splice, mounting holes, machining marks on the inner surfaces of the outer aluminum plates, locations of holes drilled into the dielectric by the contractor to probe the fields within the lenses, and the locations of the physical flaws within the lens. Some lenses showed greater uniformity than others, with fewer physical flaws. In all cases, the scans showed abnormalities, possibly air gaps, between the impedance matching transformers. On the large lens, some flaws were seen along the splice lines, between the impedance matching transformers. In addition, there was one large flaw within the interior of the lens.

All the lenses were x-rayed; however this did not reveal anything that had not been seen in the scans. Although some features were revealed with greater detail than on the ultrasonic scans, no new features were revealed. Although some details of the field probe holes and the dielectric splices show much more clearly on the x-ray, other details including the locations of possible irregularities such as air voids do not show on the radiographs.

One lens was selected for physical inspection. It was cut along a line that passed through areas of suspected flaws, and the exposed surfaces polished and examined under a microscope. Examination of the lens resulted in the verification of the ultrasonic scanning results. Air gaps were seen along the interface between the dielectric and the adhesive. For the most part, the boundary between the adhesive and the dielectric was without air gaps; however when they occurred, they were as wide as 30 microns and their locations matched the locations of the flaws on the ultrasonic scans.

Finally, in an attempt to develop an understanding of the difficulties associated with the measurement of the relative permittivity of the dielectric within the stripline structure, some measurements were made on test pieces originally used by the contractor for that purpose. The method chosen to measure the permittivity utilizes two transmission lines of different lengths, and the permittivity is determined by the comparison of signal delay or phase shift through the two lines. The method is described, and mathematical equations are derived for determining the permittivity from either the delay or the phase shift data. Next, measurements that were made on 50, 30, and 1 ohm transmission lines are described. For the measurements on 50 ohm lines, permittivity was calculated based on both delay and phase data. When compared, the average (coarse) values of the permittivity calculated by the two methods agreed when averaged over frequency, while the fine details did not. Discrepancies of up to about 10 percent were found when comparing the values obtained by the two methods. Permittivity was also calculated based on measurements of delay on the 30 and 1 ohm lines. Significant differences were found between measurements made on lines of the same impedance but from different manufacturers, and between measurements made on pairs of lines having different impedances.

It was concluded that ultrasonic tests could be used to identify surface texture, inclusions, and splices on internal surfaces or within internal layers; however it could not be used to determine at what depth or within what layer of a multilayer structure they were in. The results obtained were the same, regardless of the choice of ultrasonic frequencies. Air voids were found between the impedance matching transformers, along the dielectric splice lines, and within the central areas of some of the Rotman lenses tested. No conclusions could be made regarding the effect of the irregularities and other manufacturing anomalies on the RF performance of the lenses.

Although two similar methods of measuring the dielectric constant, based on delay and phase measurement, were used, no conclusions could be made other than the observation that the permittivity was difficult to measure accurately using the chosen method. Choice of delay line impedance affected the permittivity measured.

## CONTENTS

## LIST OF ILLUSTRATIONS

## LIST OF TABLES

## LIST OF ABBREVIATIONS

| | |
|---|---|
| BFN | Beam Forming Network |
| CTI | Chan Technologies Inc. |
| DREO | Defence Research Establishment Ottawa |
| DUT | Device Under Test |
| HP | Hewlett-Packard |
| MIC | Microwave Integrated Circuit |
| SBR | Space-Based Radar |
| μm | Micrometres |

# 1.0 BACKGROUND

## 1.1 Introduction

The Space-Based Radar R&D Project at DREO has been investigating the feasibility of the application of a number of different technologies to space-based wide area surveillance using microwave radar. In the first phase of the project, technology investigations were carried out in a variety of areas, one of which was the RF feed system. The feed system components considered were an antenna array, a receive network and a Fourier transform beam forming network. Two Fourier transform networks, a Rotman lens and a Butler matrix, were investigated. The subject of this report is the evaluation and assessment of the Rotman lenses produced under this contracted research activity. Chapter 1 contains a description of the characteristics of a Rotman lens, a historical background on the Rotman lens development for SBR, and a physical description of the SBR Rotman lenses. Chapter 2 describes the results of the physical inspection of the lenses using ultrasonic and x-ray technologies, with a metallurgical investigation to confirm the nondestructive inspection results. Chapter 3 describes measurements made on test devices to determine the effective dielectric constant of the material. The conclusions of the study are contained in Chapter 4.

## 1.2 The Rotman Lens

The design and implementation of the Rotman lens, and its utilization in antenna feed systems, has been widely described in the open literature.[1,2,3,4,5,6,7] The Rotman lens is a bidirectional electrical lens which, together with an array antenna, is capable of generating a discrete number of radiated beams simultaneously, each having a predefined direction in space. The lens consists of a parallel plate cavity region with coupling ports surrounding the cavity. There are a specified number of beam and antenna ports. Each of the antenna ports is connected to one of the elements of an array antenna by a cable of a specified length. Each beam can be formed by exciting the beam port corresponding to the desired beam. A beam is generated using the full aperture of the array and is radiated with a (sin x)/x form, with a direction proportional to the magnitude of the incremental time delay between the antenna ports, and the antenna port separation. Any combination of the available beams can be generated simultaneously by the concurrent excitation of the respective beam ports for the desired beams. Figure 1 shows a Rotman lens as it would be connected to a linear array of radiating elements. For the system illustrated, a wavefront normally incident on the array will generate an output only at beam port number 4 of the lens. Conversely, if beam port 4 of the lens is excited, the beam radiated from the array will be at broadside. Additionally, beam ports numbered 1 and 7 correspond to beams 1 and 7, at the extremes of the angular sweep of the array. The directions that the radiated beams point are frequency invariant. This wide bandwidth performance

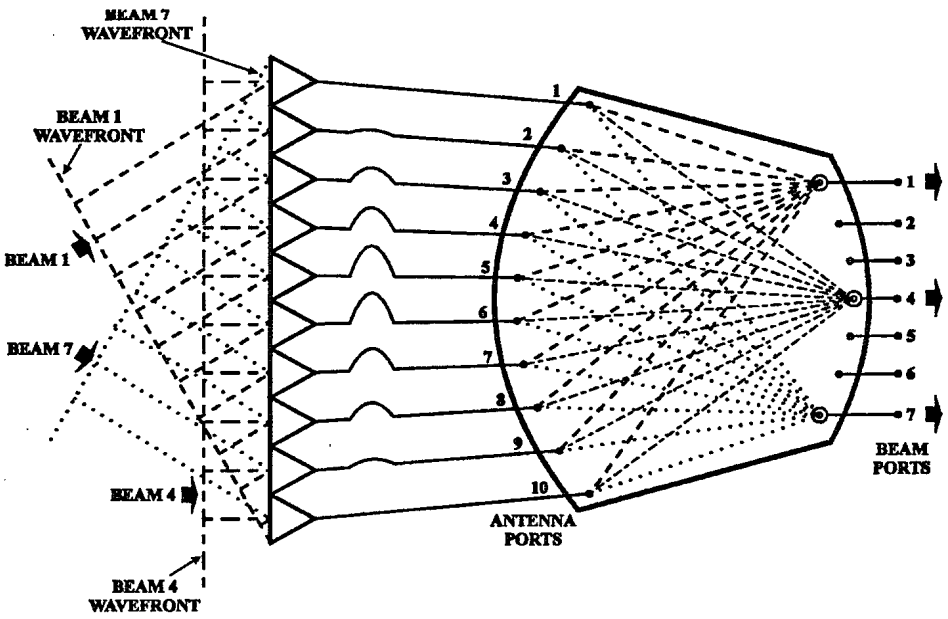


**Figure 1 Linear Array Fed by a Rotman Lens**

makes the use of Rotman lenses attractive for radar and jamming systems applications.

The Rotman lens is what is called a "true time delay" device. A different time delay is established between each beam port and each of the antenna ports. When any of the beam ports is excited, a signal of uniform amplitude is produced at each of the antenna ports. There is a progressively increasing delay between the excitation signal and the antenna port signals, depending on which beam port is being excited. The delay increment between antenna ports is a different constant for each different beam port being excited; for this reason, the beam that results from the excitation of each of the beam ports is oriented in a different direction. In Figure 1, if beam port 4 is excited, the signals at all the antenna ports will have the same delay, and thus be in phase, and the radiated beam will be normal to the array. If beam port 7 is excited, the signal radiated from antenna port 10 will have the smallest delay, while the signal from antenna port 1 will have the largest.

Another property of the Rotman lens is that the beams produced by the linear array are orthogonal to each other. These beams can be all simultaneously independently excited. If the same signal is fed simultaneously to all the beam ports, one beam will be produced for each port excitation, and the angular position of each of the beams will depend on the phase slope associated with the respective beam ports.

As noted, the antenna system has a very large bandwidth. Delays incorporated between the beam and antenna ports appear as constant delays rather than constant phase shifts. The result is that the phase shifts within the lens increase linearly with increasing frequency, and the beams generated by the phased array antenna remain stationary with frequency changes. For a phased array antenna, the phase shift per element $\alpha$ required to cause it to scan off axis to a specified angle $\theta$ is

$$\alpha = \frac{2\pi}{\lambda} d \sin \theta \qquad (1)$$

where $\lambda$ is the radar wavelength, and
$d$ is the inter-element separation.[8]

From this equation, it can be determined that if the scan angle is to remain constant as the frequency changes, the term $\alpha\lambda/2\pi d$ must remain constant. For this to happen, $\alpha$ must vary as $1/\lambda$. This will be the case if a Rotman lens, transmission lines, or some other true time delay element is used for the delay device, since the phase shift in these delay devices varies along the length $l$ as $2\pi l/\lambda$. Thus when true time delay devices are used, the antenna system bandwidth is independent of the feed network.

## 1.3 Description of Contracts for Space Feed Design and Technology Investigation

Prior to 1987, DREO technology base funded investigations were conducted in Canadian industry into technology and systems aspects related to a space-fed configuration of an antenna feed for a space-based radar. Early theoretical studies, completed in 1983, were conducted by Antech Inc. In 1985, Spar Aerospace, with assistance from Chan Technologies Inc. (CTI) and Infolytica, completed the development and testing of a C band Rotman lens in microstrip technology. In this successful development effort, CTI developed design tools based on theory of geometric optics, and designed the lens, while Infolytica performed finite element analysis. Spar Aerospace constructed and tested the lens.

In 1987, Spar Aerospace, with support from CTI, was awarded an SBR project-funded development contract, DSS Contract W8477-7-TD01/01-SV, for the design, breadboard, integration, and test of three subassemblies of the space feed of a microwave antenna system for a space-based surveillance radar. The aims of this contract were to develop the technology to implement portions of the space feed system of a space-fed phased array antenna for a proposed space-based radar, and to deliver technology demonstration proof-of-concept hardware. These subassemblies included a Rotman Lens, a Receive Beam Forming Network, and a Dipole Feed Antenna Array. Stripline technology was chosen. The summary report describes this

work.[9] This project was divided into three tasks.

1. Production of specification documents and test plans.[10] This included the conduct of a design trade-off study, the antenna design, the selection of component parameters, and the preparation of the specification and test plan documents for each of the three subassemblies and for the integrated breadboard model.

2. Design, development, implementation, and test of three subassemblies.[11,12,13]

3. Testing of the full breadboard model, consisting of the three subassemblies integrated together. In this case, a single-dimensional array of 22 dipole elements would feed a large Rotman lens, which in turn would feed a receive Beam Forming Network (BFN).

This contract was not entirely successful. The greatest difficulties were experienced with the Rotman lens development. This activity was organized into four phases:[11] the development of stripline components, the measurement of the dielectric constant of the material, the design and manufacture of 4 small Rotman lenses each having 6 antenna and 4 beam ports, and the design and manufacture of one large Rotman lens having 22 antenna and 8 beam ports. Some difficulties were experienced with the elimination of the propagation of unwanted modes and in quantifying the effects of board splices in back-to-back transitions fabricated in stripline material. The measured value of the dielectric constant varied between 10.47 and 7.6, and appeared to be a function of a number of factors. It was not possible to determine the actual value with sufficient precision to carry out a proper lens design. The performance of the four small lenses fell short of the target. Impedance matching did not meet the requirement on all the ports, and, with any of the beam ports excited, there was an unacceptable amplitude ripple between antenna ports. On the large lens, while the matching was adequate, the amplitude ripple was much worse, and the phase response was unacceptable. The poor performance was attributed to lack of precise dielectric constant data and to the presence of parallel plate modes of unknown origin within the lens that could not be coupled out using the chosen design.

Dipole arrays of 1 and 6 elements were made, and their return loss and radiation patterns were measured. A 22 element array was also designed and fabricated, and input matching checked; however its radiation pattern measurement was postponed, as it had been planned to conduct this measurement during the test of the integrated system. The results of the measurements to which the dipole elements and arrays were subjected were satisfactory, although areas where improvements could be made were identified. This portion of the contract was considered to have been successfully completed.[12]

The receive BFN was designed and developed utilizing a combination of branch line and proximity couplers. Special attention was paid to achieving high isolation, return loss, and phase accuracies in the couplers, and to the development of an excellent feed through connection for the multi-layer board. The receive BFN performed as required, with the exception of the insertion phases; it was stated that these could be corrected with adjustments to the lengths of external coaxial cables. This portion of the development was considered to be successful.[13] Because of problems encountered with the Rotman lens performance, the measurement of the integrated system was postponed until the Rotman lens could be improved.

In 1990, Spar Aerospace was awarded an extension to the previous contract to conduct an investigation into the potential causes of the failure of the Rotman lens development portion of that contract.[14] Back-to-back transitions were fabricated and small holes drilled into the top and bottom substrates so that the fields within the dielectric on each side of the copper layer could be measured using a small probe. Similar holes were drilled in the small and large Rotman lenses previously manufactured. The conclusion from the field measurements made on the back-to-back transitions was that, due to the asymmetry of the interface between the RF connector and the stripline, a portion of the power was being converted at the input connector to a parallel-plate mode within the dielectric. Because of the geometry of the connector, very little of this RF energy could be coupled out, resulting in a reduction of the output power from the lens. This was interpreted as an increase in the insertion loss of the device. In measurements made on the small Rotman lens, the phase asymmetry was found to increase with distance from the connector, indicating a difference in the dielectric constant between the top and bottom layers. The conclusion based on the measurements made on the large Rotman lens was that the major reason for the non-performance of the lens is that nearly all the power was being converted to the above-mentioned parallel-plate mode.

## 1.4 Description of the SBR Rotman Lenses

The frequency of a proposed space-based radar and the large number of radiating elements of the space feed dictated that the Fourier transform portion of the beam forming network of the feed system, consisting of two tiers of Rotman lenses, would be physically large. It was decided to implement the Rotman lenses in stripline technology.[11] Stripline construction is symmetric, with a dielectric layer on each side of a central foil circuit. The relatively large size of the Rotman lenses in the feed system combined with the limited size of the sheets of the material from which each lens would be fabricated led to the requirement that a quantity of four sheets of material would be needed in the manufacture of each side of each Rotman lens. In order to develop and evaluate the techniques for the splicing of four sheets in the production of a lens, each of the two contractors produced two small lenses, one with a splice and one without a splice, prior to the production of the large lens.

An identical lens design was used for all four of the small lenses; this design is shown in Figure 2.[9,11] Figure 3 shows the design of the large lens.[9,11] In these two cases, the external lens contour is shown along with the foil mask outline. The interior of the lens cavity has a solid copper foil mask sandwiched between the dielectric layers, with a multiple section impedance matching transformer extending to each port. On the small lens design, two 0.25 inch through holes, used to secure the lenses in the shipping container, are shown close to the edge of the lens. The cross-section of the lenses is shown in Figure 4.[9,11] The lenses are symmetric about the copper foil. A thin layer of adhesive between adjacent layers bonds them securely together. The thick aluminum plate on each exterior surface provides the required dimensional stability; as well, the inner surfaces serve as the ground plane providing the outer bounds of the lens area.

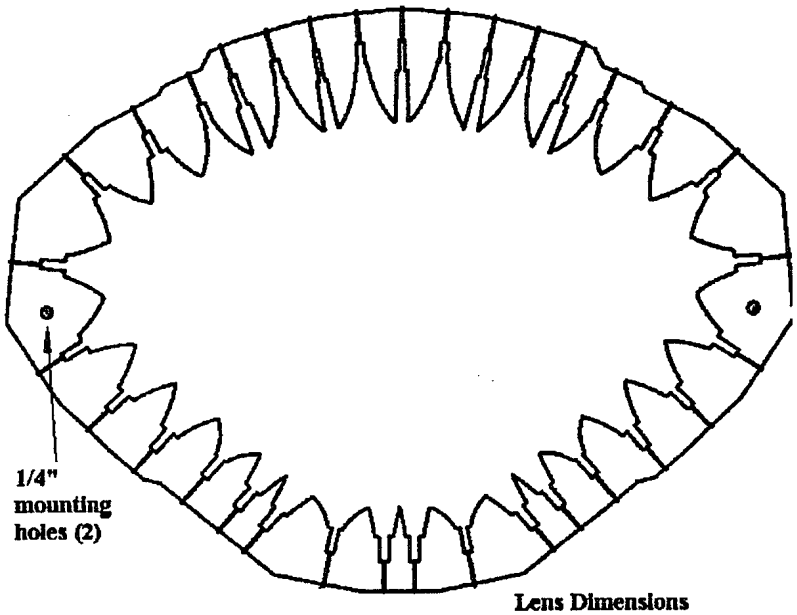


**Figure 2 Stripline Contour of Small Rotman Lens**

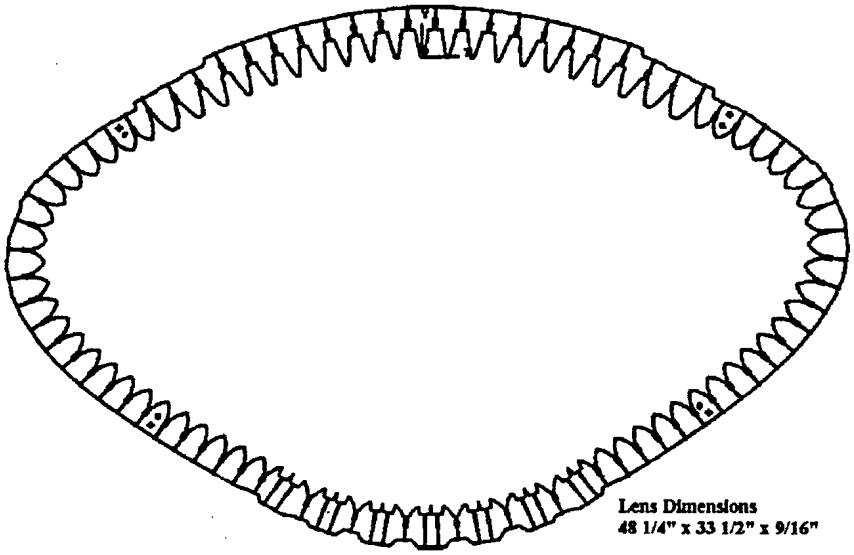


**Figure 3 Stripline Contour of Large Rotman Lens**

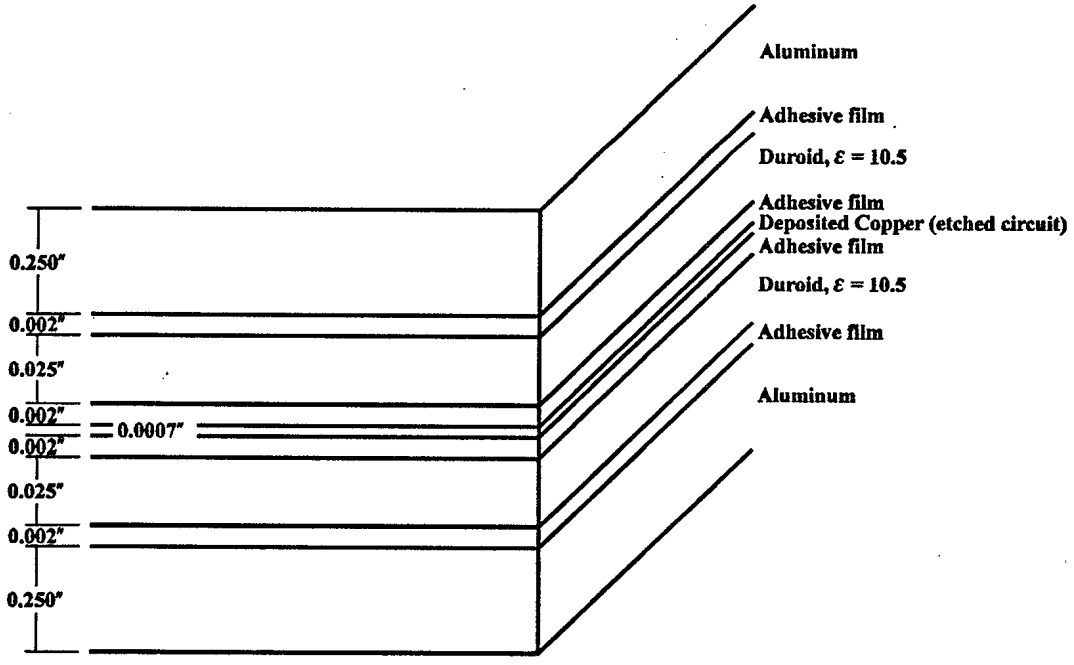


**Figure 4 Cross-Section of the Rotman Lens**

# 2.0 PHYSICAL INSPECTION

## 2.1 Introduction

This chapter details the results of the physical inspection of the four small Rotman lenses and the one large Rotman lens. The five Rotman lenses were subjected to ultrasonic scanning and x-ray evaluation in the Structures and Materials Laboratory of the Institute for Aerospace Research at the National Research Council, Montreal Road, Ottawa. Additionally, one of the lenses was sectioned to facilitate the physical inspection of the internal structure of the lens, in an effort to quantify the results of the ultrasonic inspections.

## 2.2 Non-Destructive Inspection

This section details the methodology and results of the non-destructive inspection techniques utilized to investigate the physical nature of the lenses.

### 2.2.1 Ultrasonic Inspection

#### 2.2.1.1 Introduction to Ultrasonic Inspection Methods

Ultrasonic inspection is a method of inspecting material samples without causing damage to the device under test (DUT). With this technique, beams of high frequency sound waves are introduced into the material, and the reflected waves are detected and analyzed to determine the presence and characteristics of flaws, both at and below the surface. The easiest to detect are flaws that present discontinuities between the material under test and a gas such as air. Examples of this type of flaw are open cracks, air voids, shrinkage cavities, and bonding faults.[15] Any change in the material density or the velocity of the waves will result in a reflection of some of the energy, which can be detected if the instrumentation is sufficiently sensitive.

Ultrasonic waves are mechanical waves. The frequencies used for ultrasonic inspection lie between 1 MHz and 25 MHz. They are produced by the application of high frequency electrical pulses to a transducer element which transforms the electrical energy into ultrasonic energy. When the wavelength of the ultrasonic energy is very small compared to the dimensions of the DUT, the ultrasonic energy can be directed toward the DUT and passed through it with no interference patterns resulting from internal standing waves due to the shape and size of the DUT.[16] Ultrasonic energy which is propagating through a medium is reflected at any boundary between materials which have different propagation characteristics. Because the propagation characteristics of gases are very different from those of liquids and solids, very large reflections occur at boundaries between liquids and gases, and between solids and

gases. For this reason, the energy radiated from the transducer is transmitted to the device under test through a coupling medium called a couplant. The couplant is used to eliminate any air from the space between the transducer and the DUT. The presence of a gas in this region would result in large reflections at each boundary with the gas as well as high attenuation within the gaseous medium, compared to that in a liquid. These factors would increase the sensitivity requirements for the instrumentation, as the signals from the flaws would be much smaller by the time they reached the receive transducer.

There are two common methods of conducting ultrasonic inspection. They are the contact and the immersion methods. In the contact method, the sensor is placed in direct contact with the DUT, with only a thin layer of couplant such as an oil in between them to eliminate the air gaps and bubbles, facilitating the transmission of the sound to and from the device. This is the common method used in medical diagnosis and treatment, in which a couplant is rubbed onto the skin and the sensor is moved around in contact with the surface. In the immersion method, the DUT is immersed in a liquid and the sound is transmitted through the liquid to the DUT. In this case, the sensor is placed close to, but not touching the DUT. The sound waves are conducted from the sensor to the DUT by the water. This is the most common method used for ultrasonic detection of flaws in metals.

Ultrasonic inspection is conducted by the measurement of (a) the backscatter, the reflections from the flaws and discontinuities within the DUT, (b) the transit time for the energy to pass through the DUT, or (c) the attenuation of the beam of sound waves by absorbtion and scattering within the DUT as they pass through it from one side to the other. The measurement setup for a single path attenuation measurement is shown in Figure 5a. This figure shows transmit and receive transducers, a DUT containing a flaw, and the water bath that serves as a couplant. Figure 5b shows the transmit and receive signals that would be displayed on an oscilloscope. The sensitivity of the technique, the ability to detect arbitrarily small flaws, is proportional to the frequency, while the depth of penetration is inversely proportional to frequency, and the resolution, the ability to discriminate between closely spaced flaws, is a function of pulse width.[15] The performance of the scan process can be optimized by adjusting the measurement parameters.

The data can be taken and presented in a number of ways, referred to as "A scan", "B scan", and "C scan". Each has a different method of presenting the data. In "A scan", the amplitude of the reflection is displayed as a function of time. In this case, the heights of the different vertical deflections represent the intensities of the reflections, and time translates into distance from the transducer, i.e. depth into the device being tested. Thus, for each position of the transducer, the display shows the transmit pulse, the reflection from the front and rear faces of the DUT, and if there are any flaws present, the strength of the reflection from, and depth of each of the flaws. In "B scan", the time, or depth, into the DUT is plotted as a function of position of the

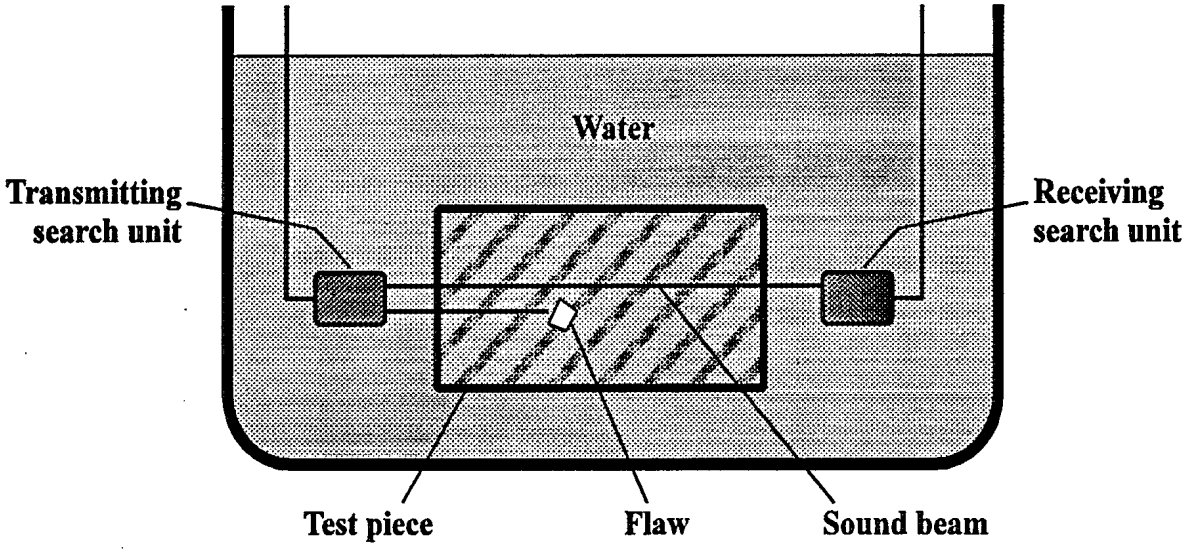


(a) Test Configuration

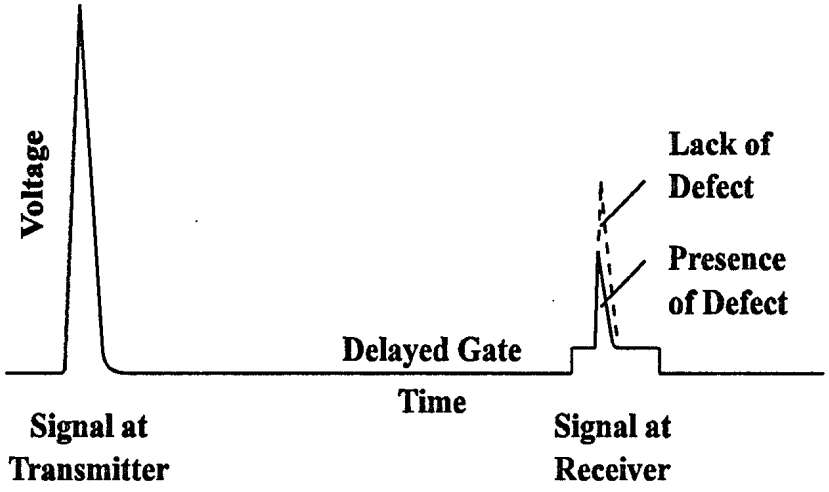


(b) CRT Display

**Figure 5. Through Transmission Test Configuration and Schematic of a Typical Oscilloscope Display**

transducer along a line on its surface. Echo intensity is not measured, but is represented by the relative brightness of the echo indications on the display.

The third scan type is "C scan". In this scan type, the response is shown as a function of position within an area, a plan view presentation. This response can either be reflections from the flaws or the transmission attenuation. The depth of the flaws is not usually recorded or displayed, as the two axes of the display are utilized to provide the rectangular coordinates of the DUT. The display shows the relative physical size of each reflection, while the strength of the reflections are represented by the relative brightness of the echo indications on the display. To obtain a transmission attenuation profile of the device, the transmitting and receiving transducer probes are physically scanned over the surface of the DUT, producing a two dimensional view of the transmission characteristics. Areas having different transmission attenuation can be seen as areas of differing densities. The presence of flaws or voids is indicated by areas of higher attenuation; these are detected and mapped as two dimensional colour images. Although the size and location of the flaws in the planar view is indicated, their depth or thickness cannot be determined. When using this technique, usually only the signals reflected from within the DUT are gated into the receiver, eliminating the strong reflections from the front and rear surfaces of the DUT. The C-scan technique is sensitive to flaws such as cavities, disbond between layers, and material inhomogeneity.

#### 2.2.1.2 Results of the Ultrasonic Scanning of the Rotman Lenses

This section details the results of the scanning of the lenses.[17] The immersion technique was used to facilitate the production of C scan images of the attenuation of ultrasonic waves at frequencies of 5, 10, 15, and 25 MHz as they passed through the lenses from top to bottom. First two lenses were scanned to evaluate the process, followed by the detailed scanning of all the lenses at each measurement frequency. Table 1 shows the ultrasonic scanning measurements that were made on each lens.

Lenses A and B were selected for preliminary assessment using ultrasonic scanning technology. This preliminary scan was performed to evaluate the feasibility of utilizing ultrasonic scanning to determine the internal structure of the lens. Of concern was the possibility that the ultrasonic energy would be unable to penetrate the thickness of the lens, or for some other reason be unsuitable for this application. From the results of the preliminary scan, there was no evidence to indicate that the ultrasonic scanning technique could not be applied to these investigations. All four small lenses were then individually scanned. In each case, the lens was measured at frequencies of 5, 10, 15 and 25 MHz. The use of different measurement frequencies increases the possibility of finding additional features; at high frequency there is an increased sensitivity and thus a chance of finding smaller features.[15] Results are discussed below.

**Table 1. Ultrasonic Scanning of Rotman Lenses**

| Lens | Description | Testing |
|---|---|---|
| A<br>NRC #1 | Lens by CMR, Montreal<br>Single Board Construction<br>(No splice) | Preliminary Scan: 5 MHz<br>Final Scan: 5, 10, 15, & 25 MHz<br>(Figs. 6, 7, 8, 9) |
| B<br>NRC #4 | Lens by Buckbee-Mears,<br>St. Paul, MN<br>Single Board Construction<br>(No splice) | Preliminary Scan: 5 MHz<br>Final Scan: 5, 10, 15, & 25 MHz (5 MHz - Fig. 10) |
| C<br>NRC #3 | Lens by CMR, Montreal<br>4-Board Construction (Spliced) | Final Scan: 5, 10, 15, & 25 MHz (5 MHz - Fig. 11) |
| D<br>NRC #2 | Lens by Buckbee-Mears,<br>St. Paul, MN<br>4-Board Construction (Spliced) | Final Scan: 5, 10, 15, & 25 MHz (5 MHz - Fig. 12) |
| Large<br>NRC #5 | Lens by Buckbee-Mears,<br>St. Paul, MN<br>4-Board Construction (Spliced) | Final Scan: 5, 10, 15, & 25 MHz<br>(Figs. 14, 15, 16, 17) |

Figure 6 shows the results of the scan of lens A at 5 MHz. The lens outline can clearly be seen. The vertical lines are evidence of machine work on the aluminum plate prior to assembly. These result from overlap during milling operations, performed to flatten the inner and outer surfaces of the 0.25 inch thick aluminum ground planes. This machine work can be seen on examination of the external surfaces of the lens; however it is the reflection from the internal surfaces that is producing this feature on the display, because the reflections from the outer surfaces have been gated out during the scan analysis. In addition, this was confirmed by the comparison of scans of this lens, both before and after the polishing of its external surfaces to remove the blemishes and surface texture. The blotching is caused by the texture of surface imperfections at one or both of the internal surfaces. By comparing with Figure 2, one can see that dark areas close to the outer edge of the lens lie between the impedance matching transformers. These areas may possibly be air bubbles which were trapped between the adhesive layers, held apart by the adjacent copper foil during manufacture, or adhesive which flowed there while the lenses were being heated under pressure during manufacture. There is also evidence of abnormalities along the vertical milling overlap lines because of areas of increased

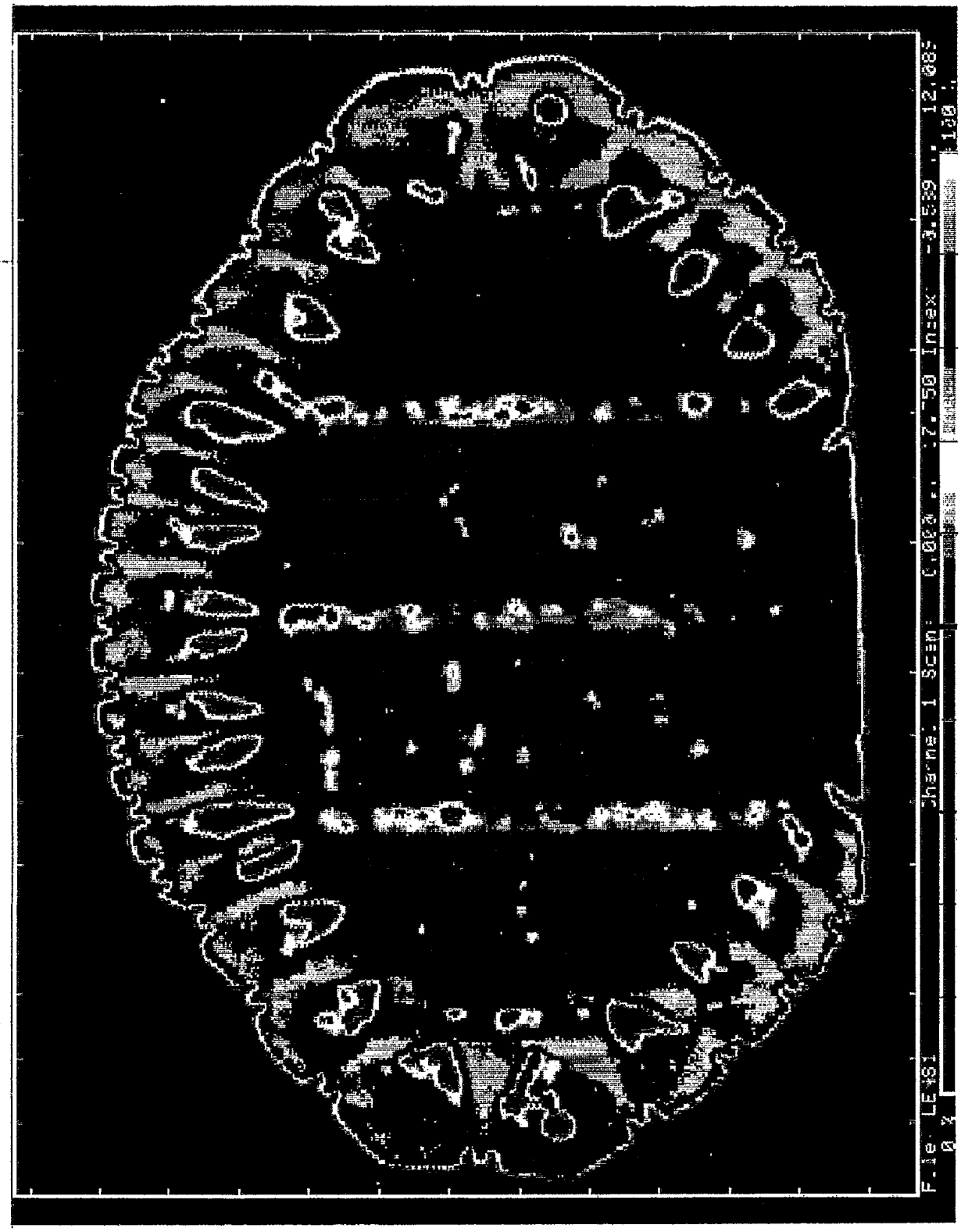


**Figure 6 Final Scan of Rotman Lens RL 1.10A at 5 MHz Single Board Construction (Not Spliced)**

density similar to those between the matching transformers.

By comparing the data in Figures 6 to 9, using Figure 2 as a guide, it is evident that the primary features, the mounting holes, the possible air gaps between the matching transformers, many of the stronger reflections from internal irregularities, and the milling overlap lines remained unchanged when the transducers were changed and measurements were taken at other frequencies. The "clutter" and overall brightness differences are partly due to the difference in the sensitivity of the sensors.[17] When each of the Rotman lenses was scanned, little new evidence of additional features was seen when the probing frequency was changed. The external surface of lens A was clean, without field probe holes. With the exception of the possible cavities along the milling overlap lines and between the matching transformers, the lens appears to be well bonded and of relatively clean construction.

Figure 10 is the result of the scan of lens B. The results are similar to those in Figure 6; the principal differences are that the lines from the machine work on the aluminum plate are across the wide dimension of the lens rather than across the narrow one, and evidence of possible air gaps along the milling overlap lines is not so strong. Although measurements were made at all four frequencies, only the result for 5 MHz is shown because of the similarity of the results. As above, using Figure 2 as a guide, it again can be seen that there are likely cavities between the matching transformers, and that the image of each of the two 0.25 inch mounting holes has been merged with one of the inter-transformer irregularities. The milling overlap lines are barely visible. With the exception of the above comments, this lens appears to be exceptionally clean and free of internal anomalies.

The scan of lens C for 5 MHz is shown in Figure 11. As above, the results of the measurements at all the frequencies were similar, so only one result is shown. Evidence of possible voids can be seen between all the matching transformers, along the milling overlap lines, and scattered throughout the body of the lens. In lenses C and D, field probe holes were drilled from each side through the external aluminum plate into the dielectric layer to allow a small probe to be inserted for measuring electromagnetic wave propagation within the lens. Figures 11 and 12 showing the scan data can be compared to the scale drawing in Figure 13 for location of the 1/4 inch mounting holes, the dielectric splice and the field probe holes. The field probe holes appear oval on the scans because the image of each hole represents both that of the hole and the two adjacent screw mounting holes, and these individual features could not be resolved by the scan process. A detail of this is also shown in Figure 13. Twelve holes were drilled in each side of the lens, in four sets of three. Each set lies along a line between the centre of the lens on the beam port side and the antenna port side. A very wide region of suspicion surrounds both axes of the splice, with an apparent opening at each end of each axis. This may indicate some problem during manufacture.

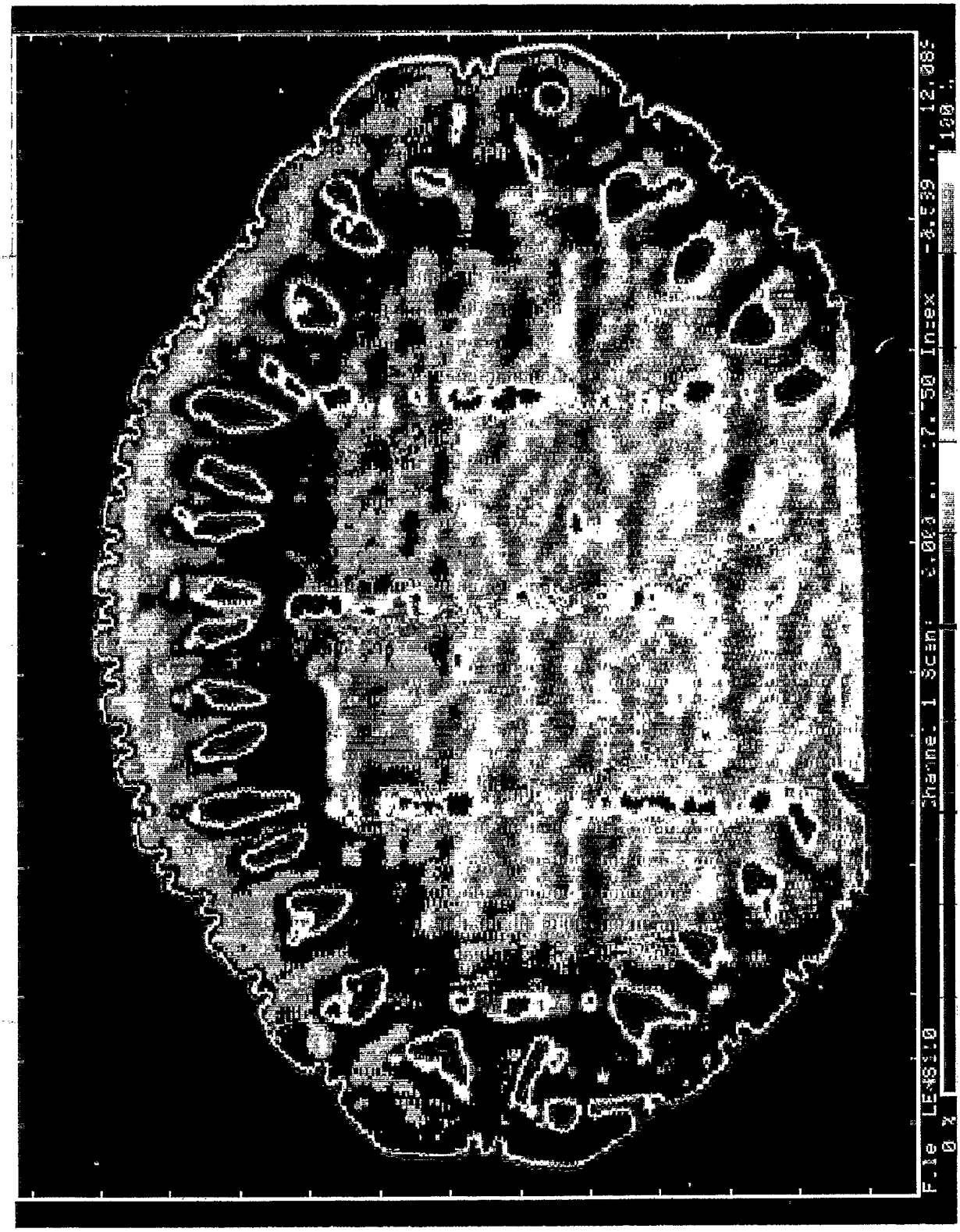


**Figure 7 Final Scan of Rotman Lens RL 1.10A at 10 MHz Single Board Construction (Not Spliced)**

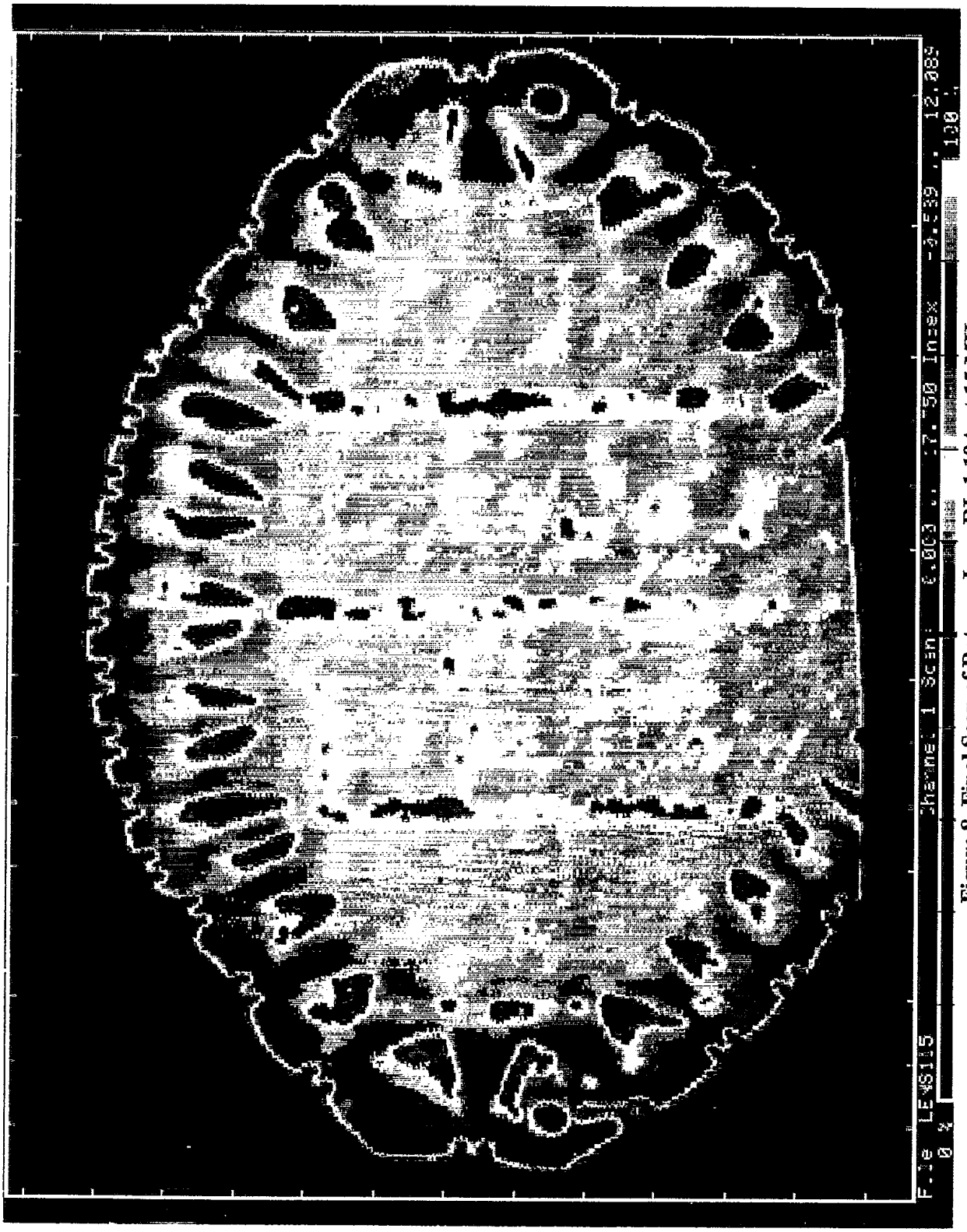


**Figure 8 Final Scan of Rotman Lens RL 1.10A at 15 MHz Single Board Construction (Not Spliced)**

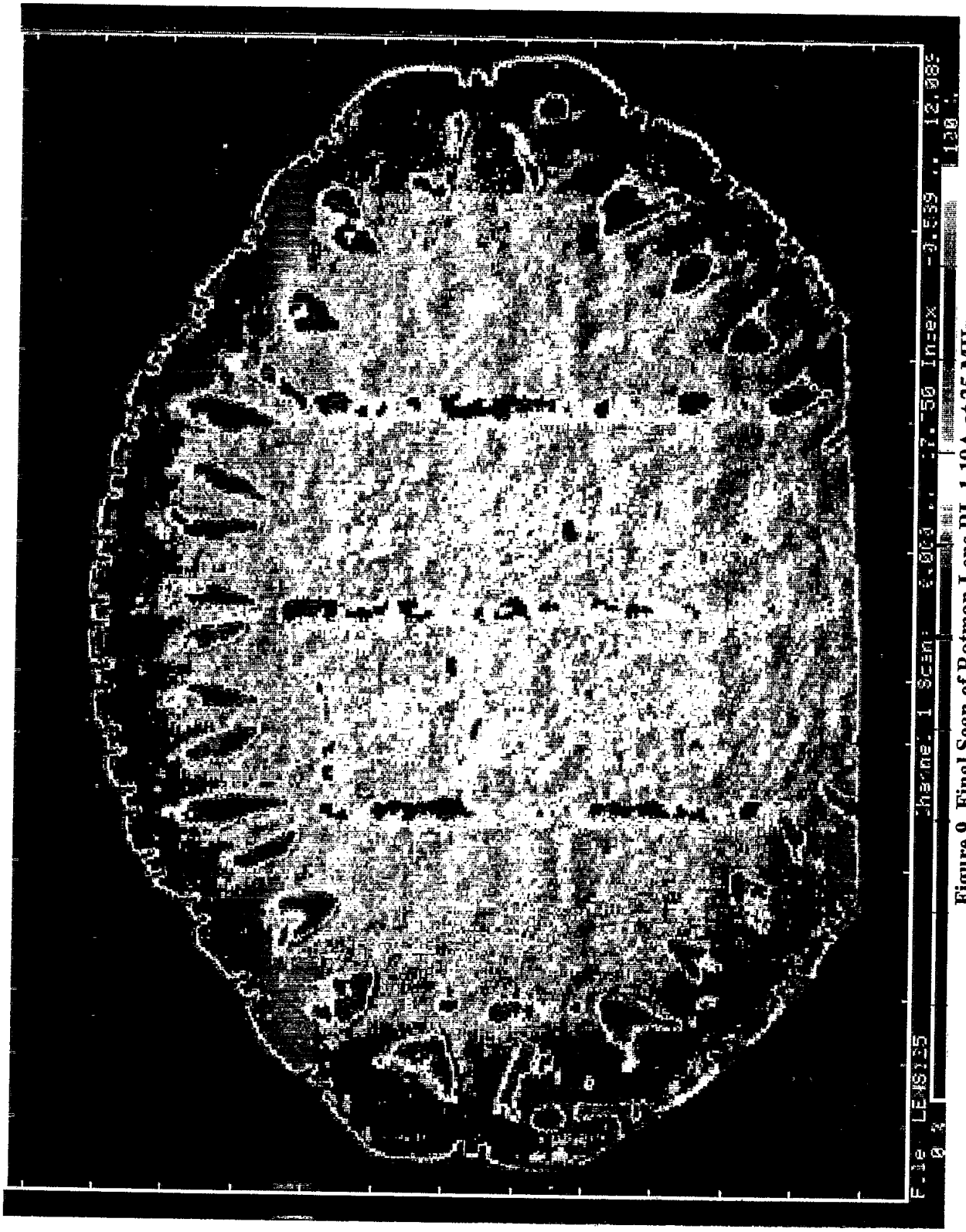


**Figure 9 Final Scan of Rotman Lens RL 1.10A at 25 MHz Single Board Construction (Not Spliced)**

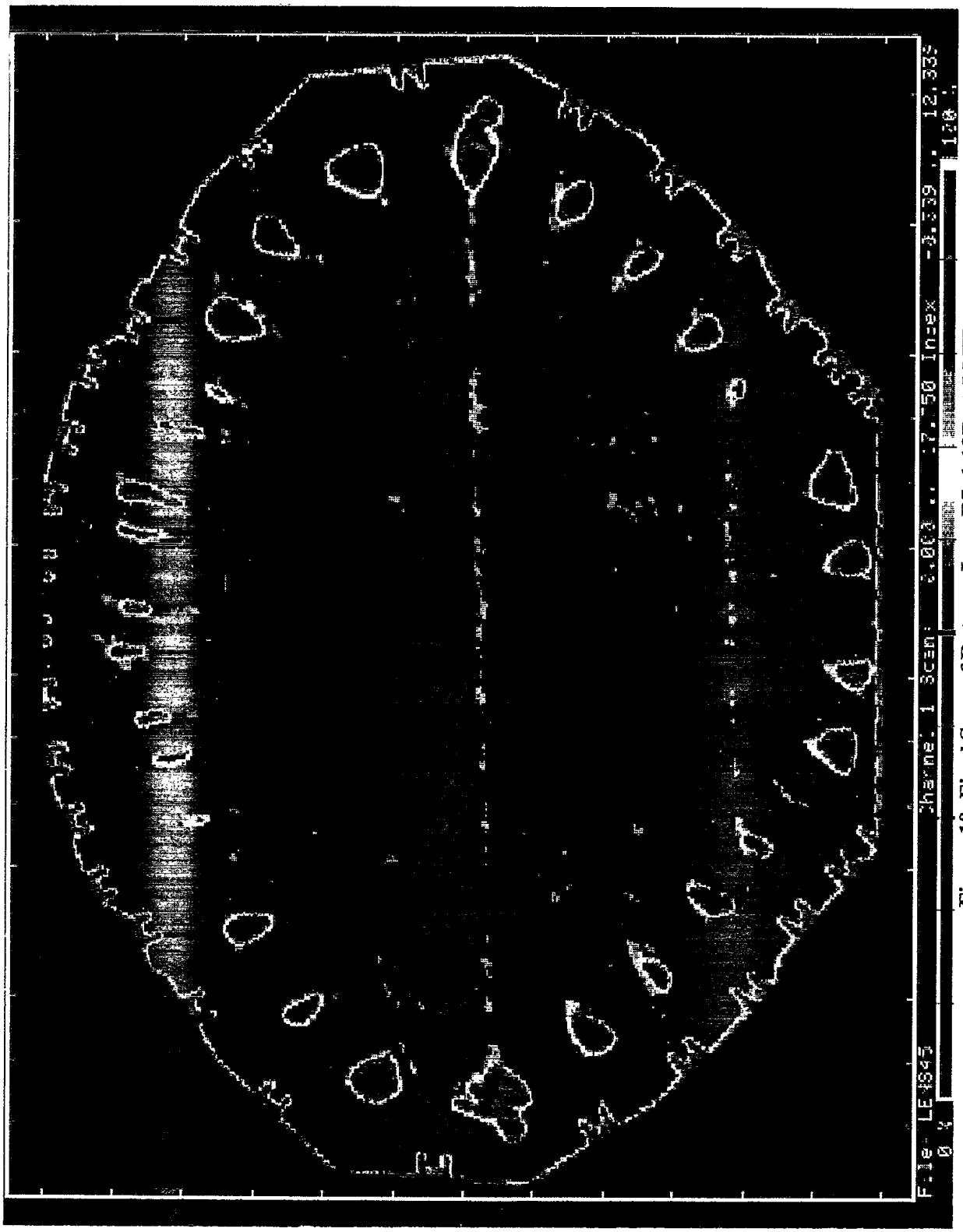


**Figure 10 Final Scan of Rotman Lens RL 1.10B at 5 MHz Single Board Construction (Not Spliced)**

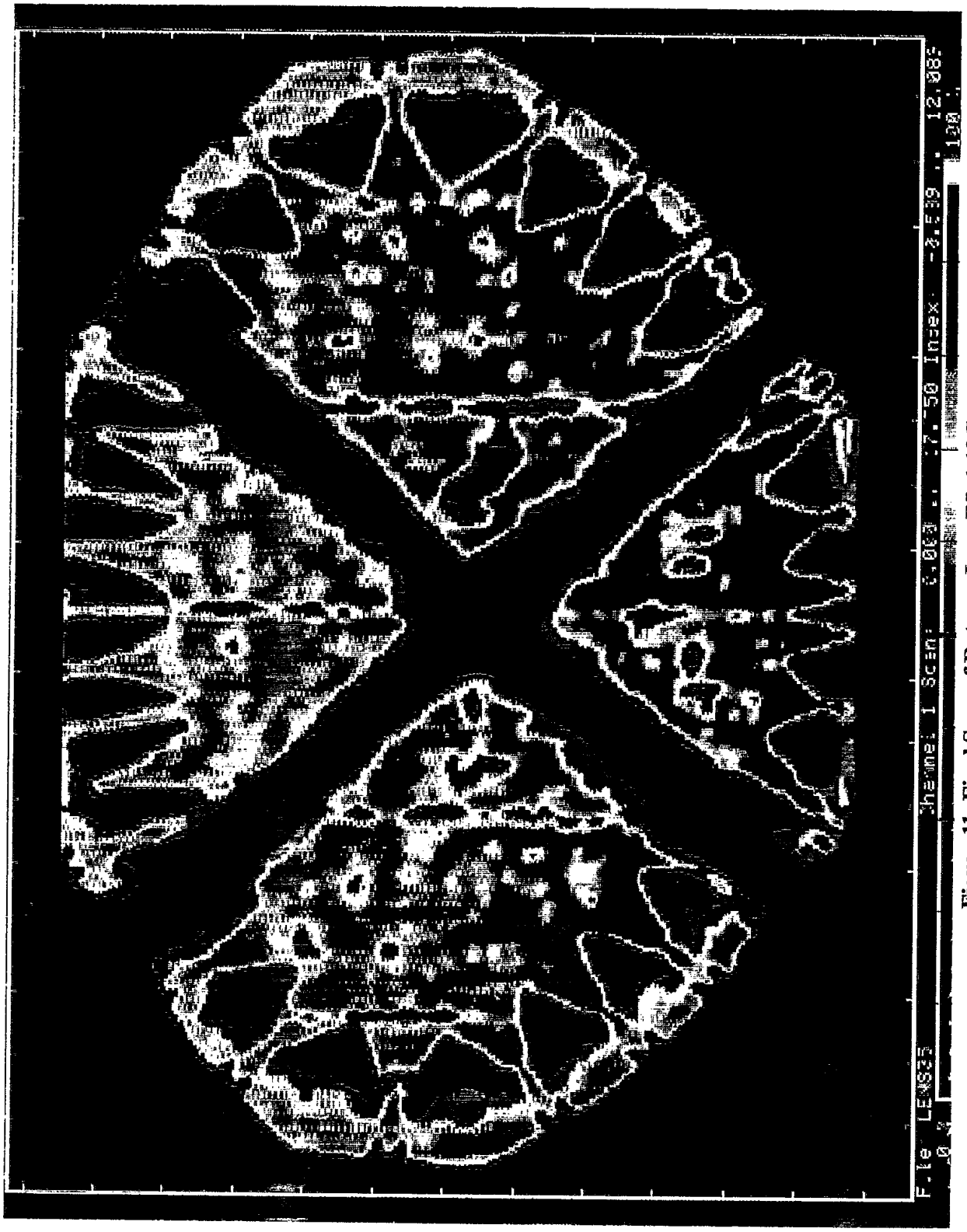


**Figure 11 Final Scan of Rotman Lens RL 1.10C at 5 MHz Four Board Construction**

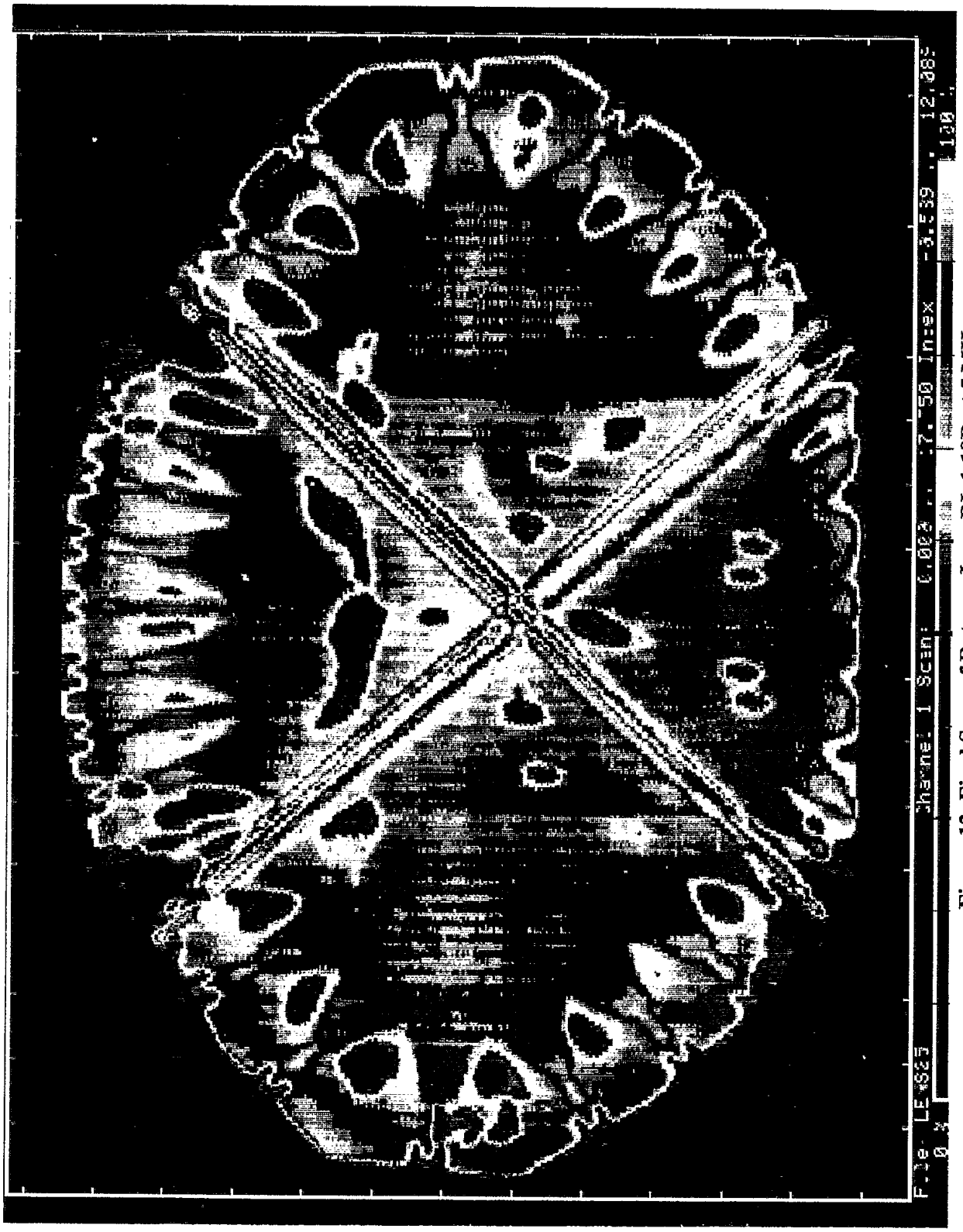


**Figure 12 Final Scan of Rotman Lens RL 1.10D at 5 MHz Four Board Construction, Polished**

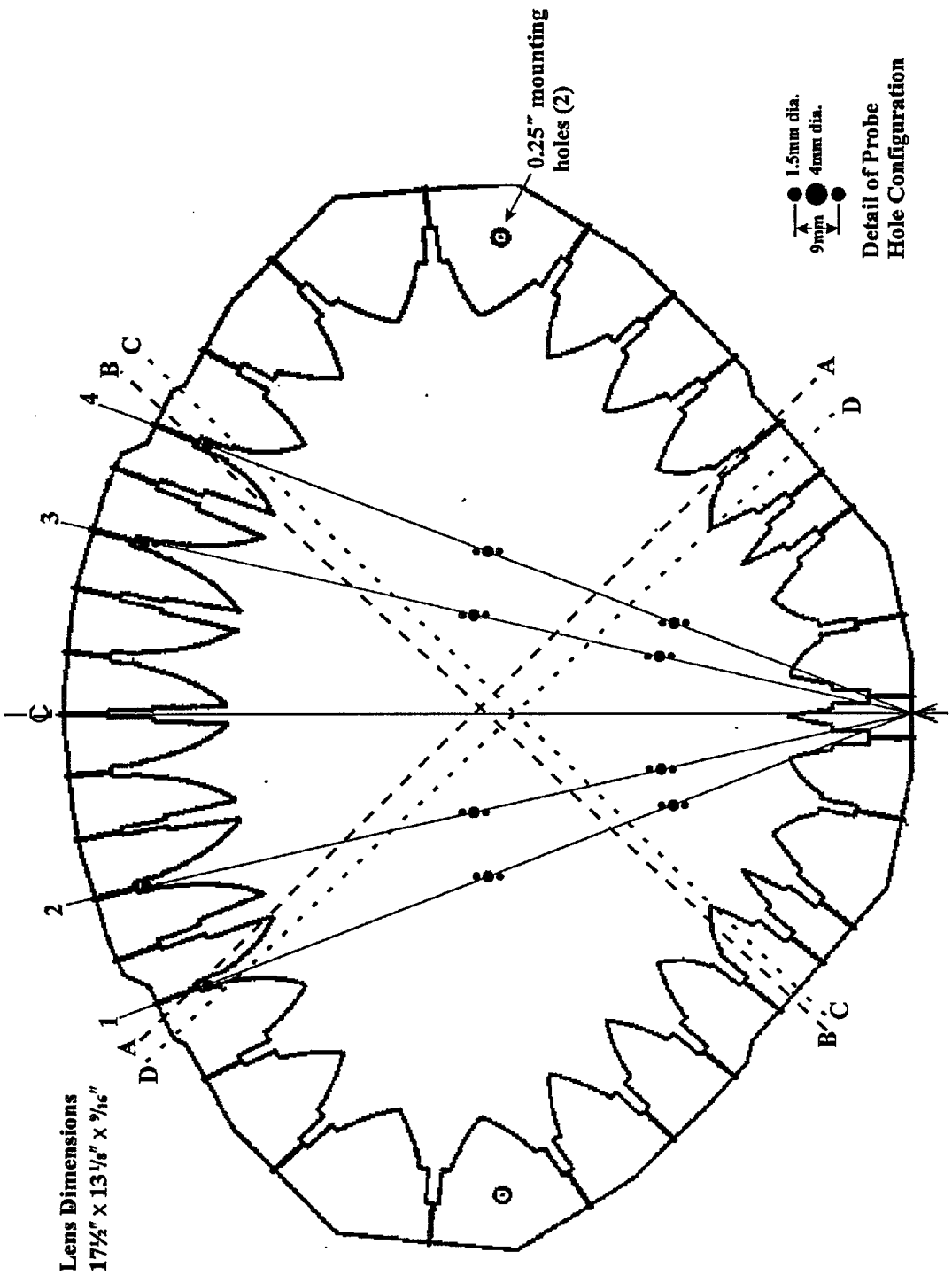


Figure 13 Stripline Contour of Small Rotman Lens Showing Location of Field Probe Holes and Dielectric Splice.

Figure 12 shows the results of the scan of Lens D for 5 MHz. As above, only the one result is shown because of the similarity of the results at the different frequencies. By comparing the scans to Figure 13, the locations of some of the field probe holes can be identified. The holes closest to the beam port side and toward the centre of the lens can be readily located. The holes closest to the antenna ports in each of the sets are difficult to locate because they are hidden by the anomalies at the edge of the lens. The milling overlap lines, vertical in this case, can be seen, but are not dominant. The splices are clearly visible, forming two "X" shaped crosses on each of the scans. It is assumed that the splice in each layer will have the same colour on the C-scan; splice A-B is pink in the scans and splice C-D is red. There is a misalignment between the splices in the upper and lower layers. Several significant suspect areas can be seen in the interior of the lens adjacent to the dielectric splice, and there appears to be some sort of irregularity in the lens at each end of each dielectric splice. Possible cavities between the matching transformers are also evident in the scan of lens D, and the image of each of the two 0.25 inch mounting holes has been merged with the returns from anomalies between adjacent output transformers.

The scans of the large Rotman lens are in Figures 14 to 17. Significant potential voids can be seen, primarily along the splice lines, between the impedance matching transformers, and in one other area. Eighteen field probe holes were drilled along three lines on each side of the lens, extending from the beam port side to the antenna port side. Those closest to the beam port side are close together, and cannot be resolved. The third hole in the first set lies on a splice line and cannot be resolved, and the furthest holes lie between impedance matching transformers, and can be found by careful inspection due to their characteristic shape. The location of the probe holes and the splices is indicated in Figure 18.

It was desired to determine the depth of the texture created by the milling operation when the 0.25 inch thick aluminum plates were flattened. It is suggested that during manufacture, the milling overlap areas and other depressions in the surface could trap additional adhesive or air. Since the dielectric constants of the dielectric, the adhesive, and air are 10.5, approximately 4.0, and 1.0 respectively, the presence of air or varying thicknesses of adhesive may affect the overall dielectric constant of the dielectric, causing measurable deviations in the RF performance. On the assumption that the inner and outer surfaces of the cover plates of the lenses are identical, the external milling overlap lines have been examined on lenses B and C. Using a microscope to measure the difference in surface heights, these overlap lines have been found to be depressions of typically up to 0.0006 inches in depth. This is consistent with production tolerances which required flatness to within .001 inch.[18] Lenses A and D could not be examined because the external surfaces have been polished smooth. According to the design documents,[11] each adhesive layer is 0.002 inches thick, about three times the depression depth mentioned above.

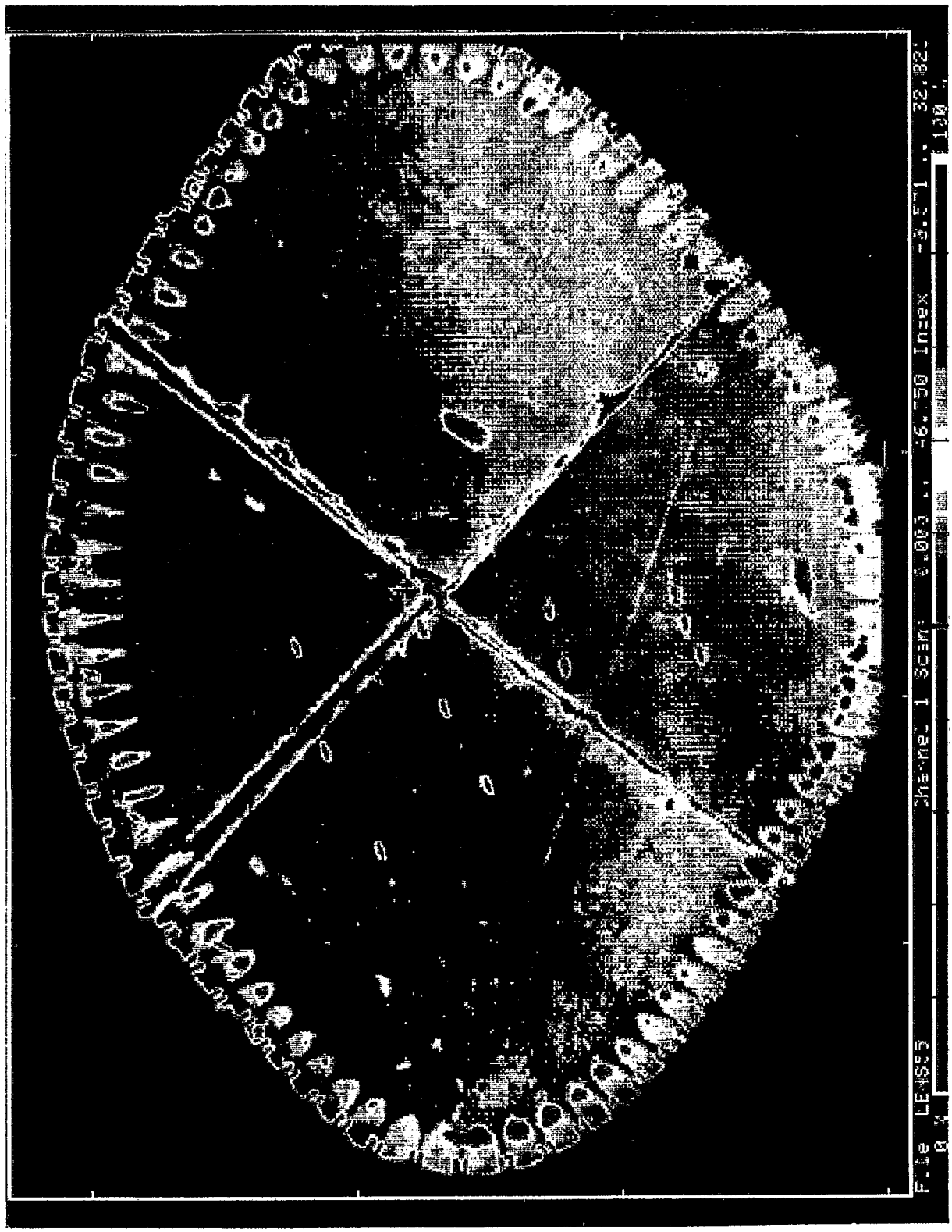


**Figure 14 Final Scan of Large Rotman Lens at 5 MHz**
**Four Board Construction, Not Polished**

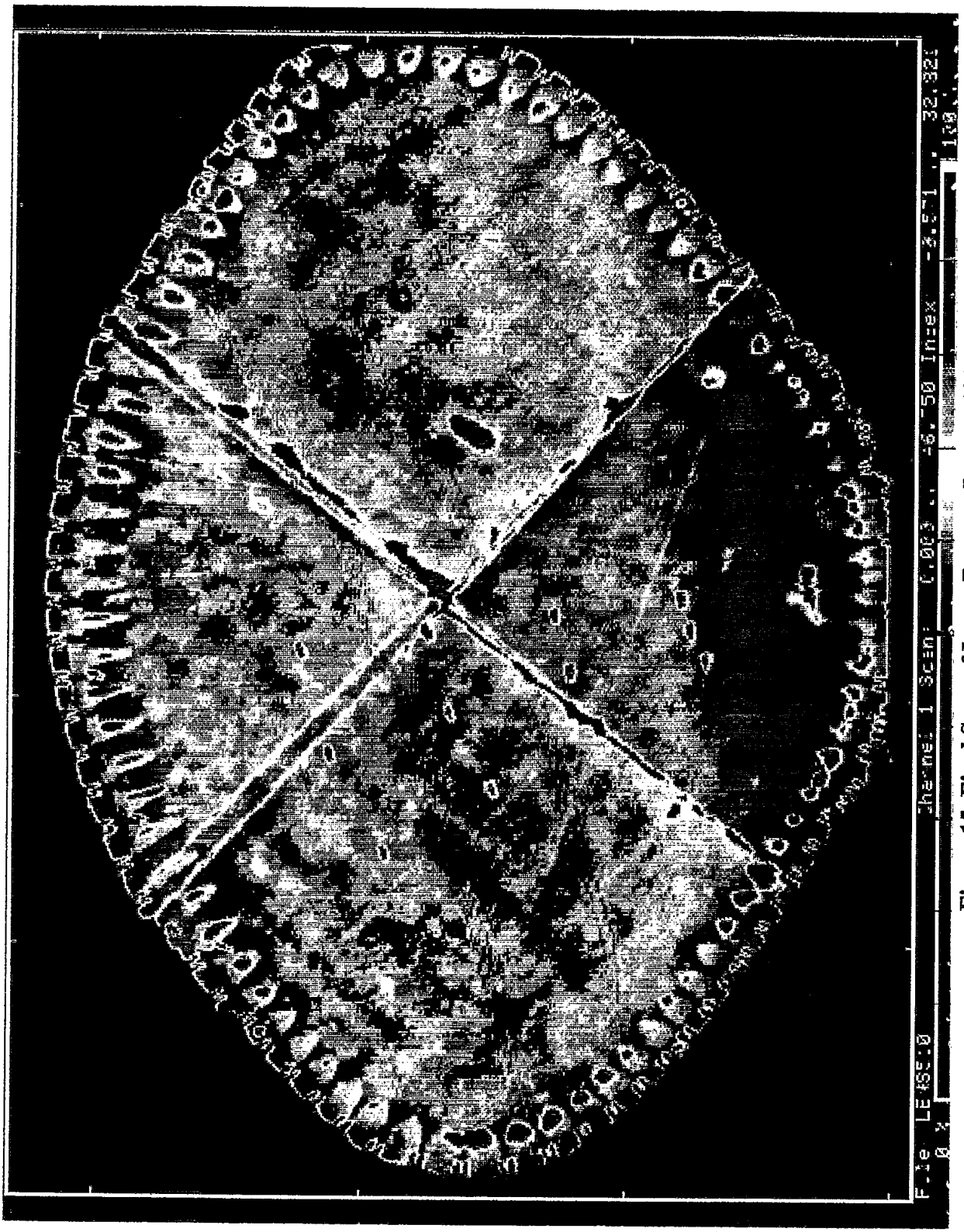


**Figure 15 Final Scan of Large Rotman Lens at 10 MHz**
**Four Board Construction, Not Polished**

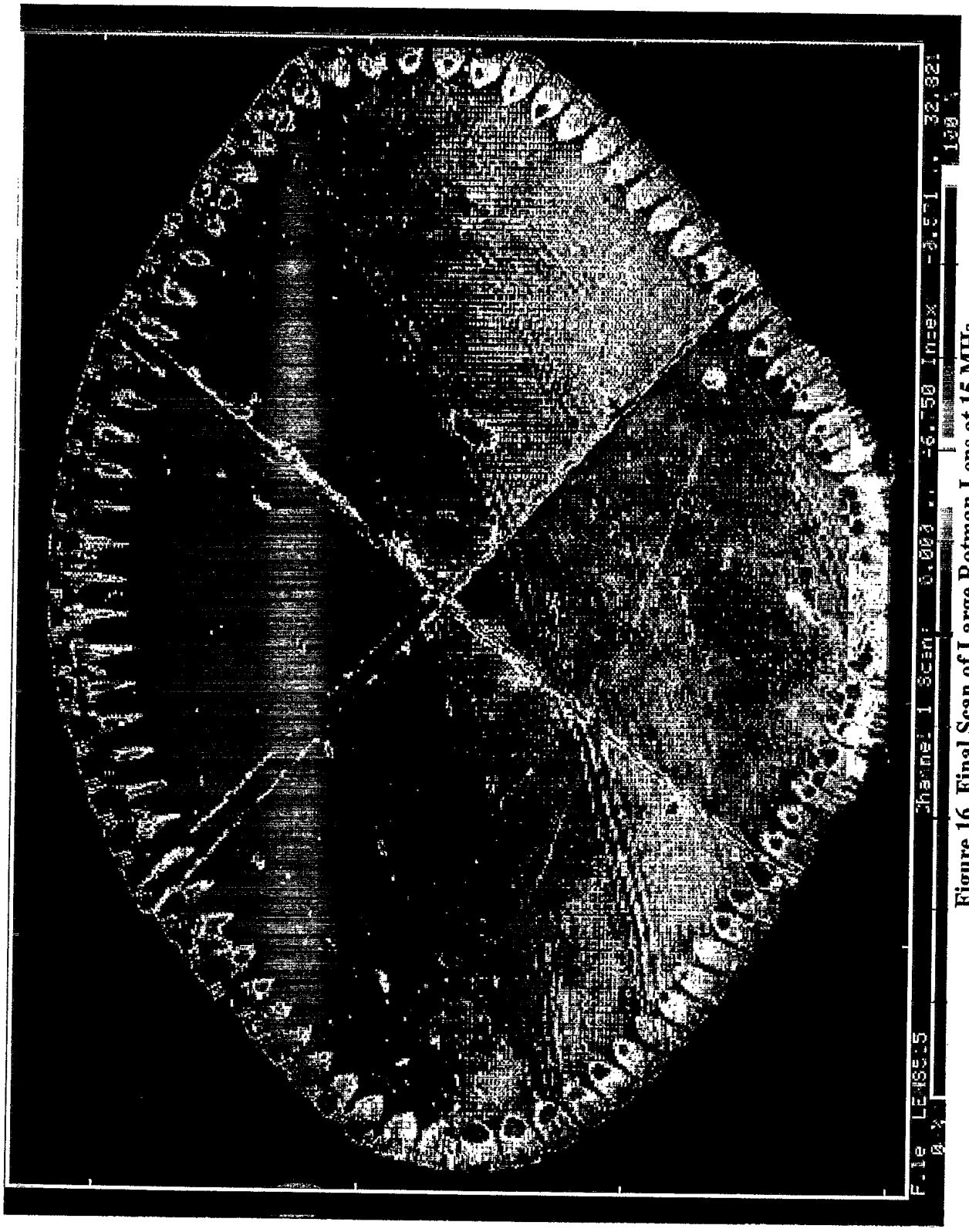


**Figure 16 Final Scan of Large Rotman Lens at 15 MHz Four Board Construction, Not Polished**

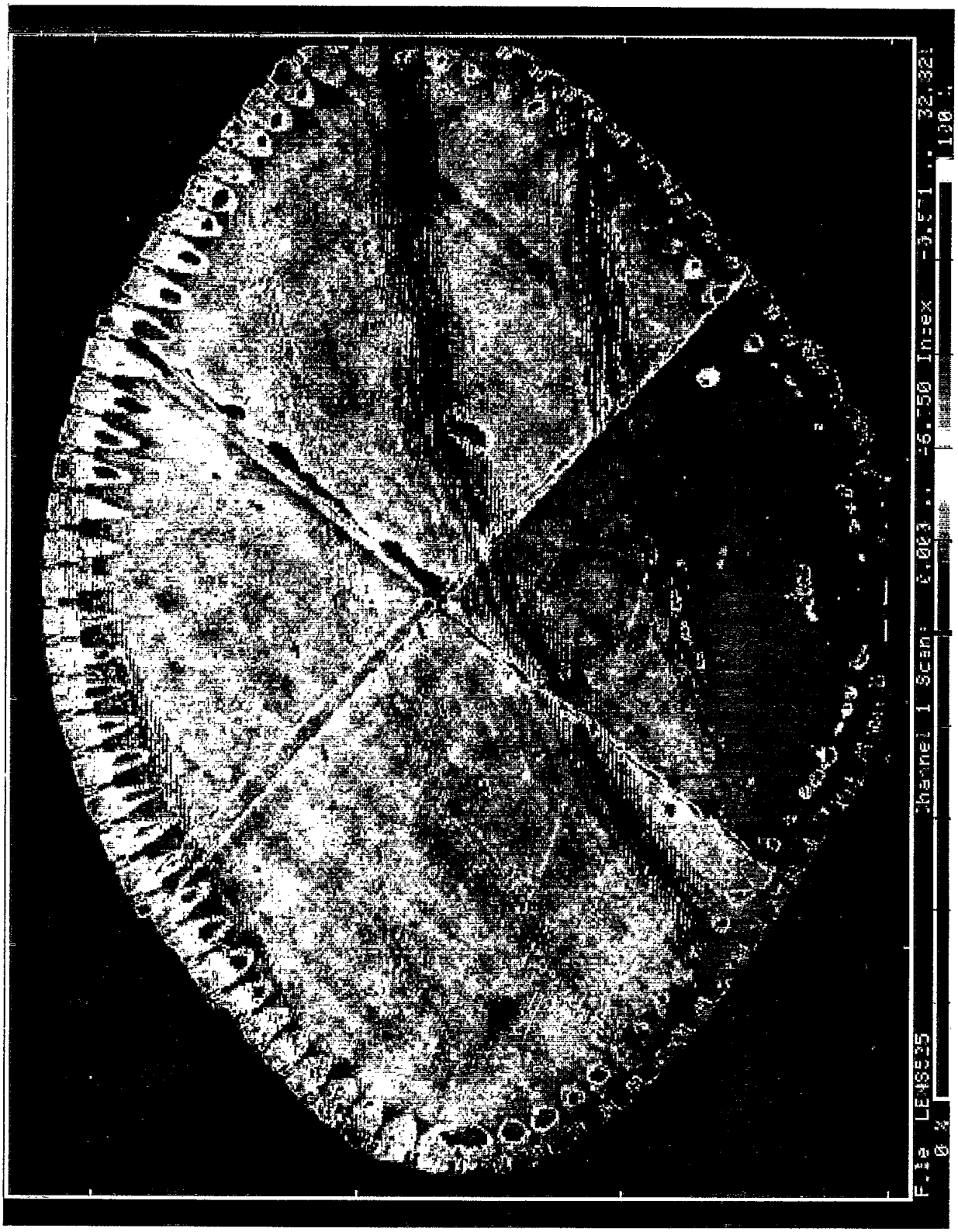


**Figure 17 Final Scan of Large Rotman Lens at 25 MHz**
**Four Board Construction, Not Polished**

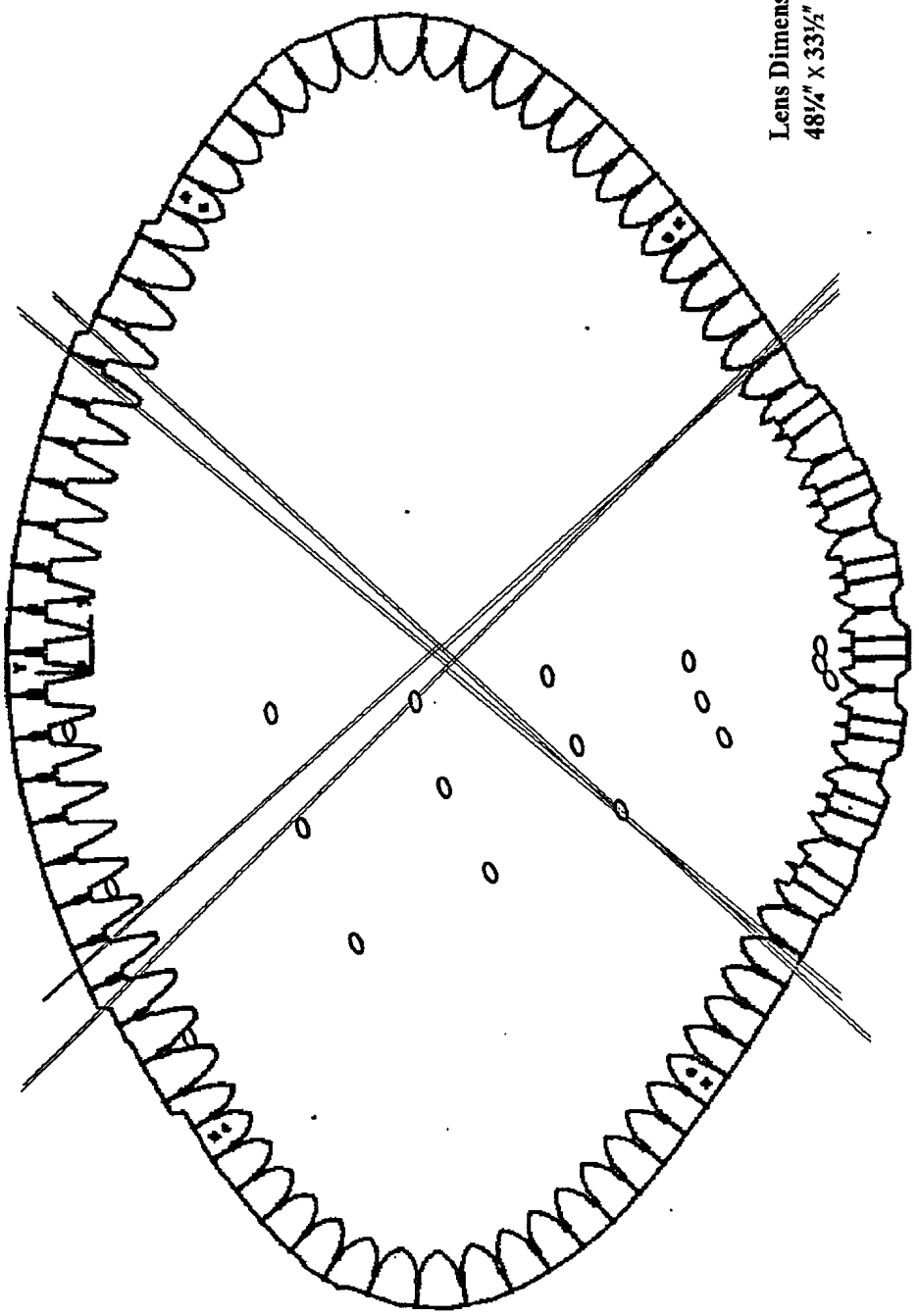


Figure 18 Stripline Contour of Large Rotman Lens Showing Location of Field Probe Holes and Dielectric Splice.

### 2.2.2 X-Ray Inspection

In order to provide additional insight into the internal structure of the lenses, each lens was also probed using x-rays. In a manner similar to the C-scan, X-radiography provides a two-dimensional picture of the intensity distribution of X-rays that have passed through the test object. This type of testing is most sensitive to variations in specimen density or the presence of flaws of different densities. Particularly, internal flaws such as porosity, cavities, cracks, inclusions of different densities, and material inhomogeneity are most easily detected by X-rays, while delamination or disbond between layers are more easily detected using ultrasonics. In this manner, X-ray and ultrasonic testing methodologies are complementary.[17] A single radiograph was made for each of the small lenses, while the large lens required 8 separate frames because of its size.

A sample x-ray from one of the small lenses is shown in Figure 19. It has been inverted to make it consistent with the scan photos and other drawings for easier comparison. Clipping of the image at the edges resulted because the x-ray film material was slightly smaller than the lens. Lens D was chosen because it contains all the possible features. The outline of the lens is shown along with the RF connectors attached. The two white lines under each of the connectors are the tapped holes for the connector mounting screws. The foil mask outline can easily be seen, including the impedance matching transformers. The figure shows the splices in the top and bottom layers; it can be seen that they are misaligned from one another. The two 0.25 inch alignment holes are evident at the horizontal extremes of the lens. Twelve field probe holes per side are shown. With each is a pair of tapped mounting holes for holding the probe in place during the field measurement process. There is very little blurring of the field probe holes, indicating good alignment between the holes in the top and bottom layers. It can be seen that these radiographs provided little information in addition to that which was already available from the ultrasonic scans. Although the details of the field probe holes and the dielectric splices show much more clearly on the x-ray, the other details, including the locations of possible irregularities such as air gaps do not show on the radiographs.

## 2.3 Metallurgical Inspection

The results of the ultrasonic scanning of the Rotman lenses revealed, in some cases, areas that aroused suspicion due to the high attenuation of ultrasonic energy. The ultrasonic testing revealed qualitative results only, and provided no insight into the real cause for the areas to be identified. A number of possible causes were postulated; included among these were areas of additional thickness of adhesive, and the presence of trapped air bubbles between the layers. One possible way to detect the real cause of the anomalies in the ultrasonic scans was to cut one or more of the lenses and examine the cross-section for defects. In this way, the thickness and nature of the

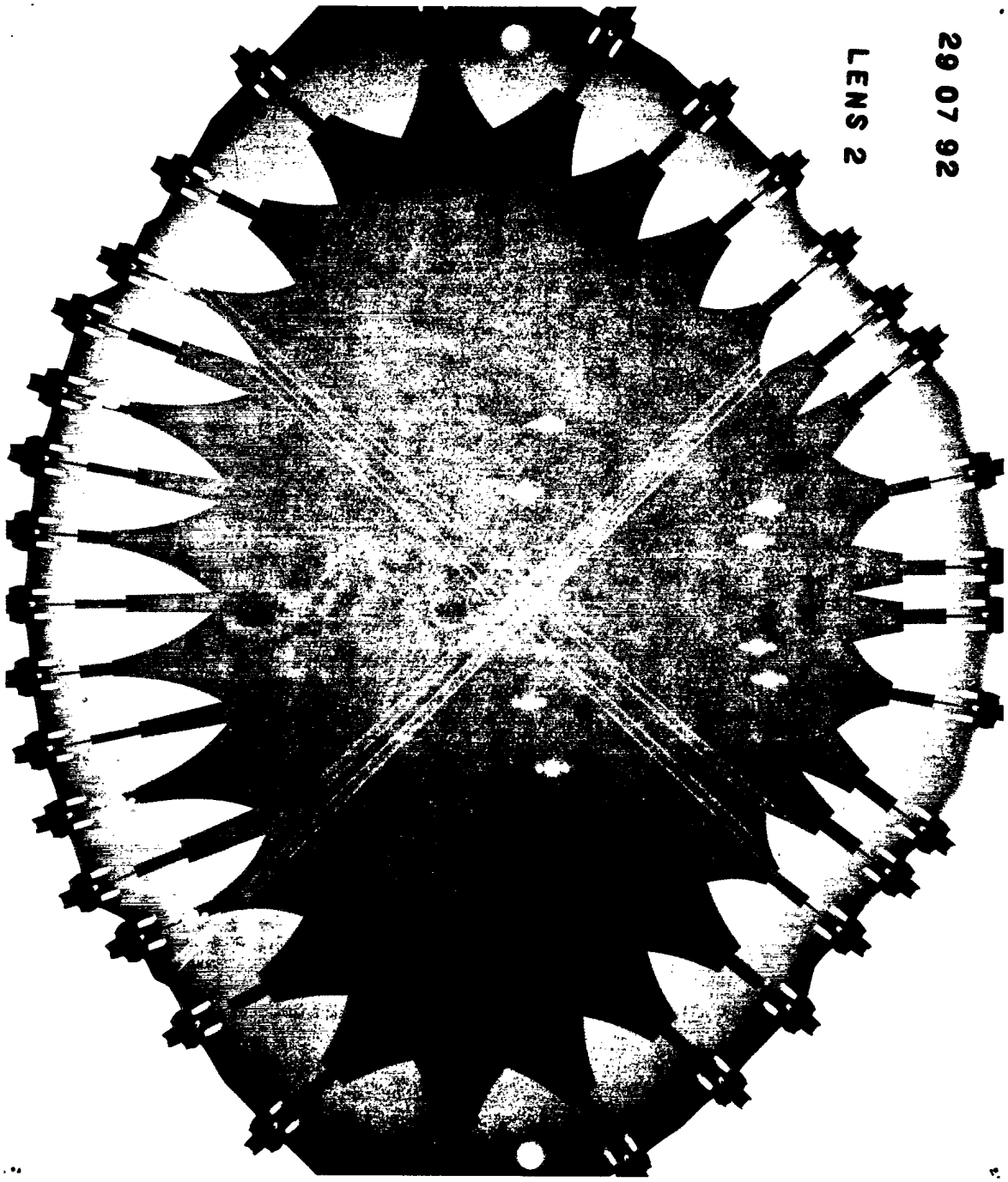


Figure 19 X-Ray of Rotman Lens RL 1.19D
Four Board Construction

defects could be determined.

Lens C was selected for destructive inspection. Spar Aerospace had communicated to DREO that they believed that the results of the C-scans could have been influenced by the resonance of the finite structure. In order to confirm or deny this possibility, a single cut was made close to one edge in order to destroy the structural symmetry of the lens. The lens was subsequently scanned and the new scan compared to the original scans. No noticeable differences in the scans of the lens were found; all important anomalies were still present, suggesting that resonance did not occur.[17] It was thus concluded that the original scans represent the internal structure of the lenses.

Following the verification of the integrity of the scanning process, an additional cut in the lens was made. The locations of the two cuts are shown in Figure 20. The narrower vertical cut on the left was made for the verification of the integrity of the ultrasonic scanning process, described above, and the wider vertical cut on the right was for producing the specimens for examination. The "X" shaped pattern in the centre of the lens is the discontinuity associated with the splice.

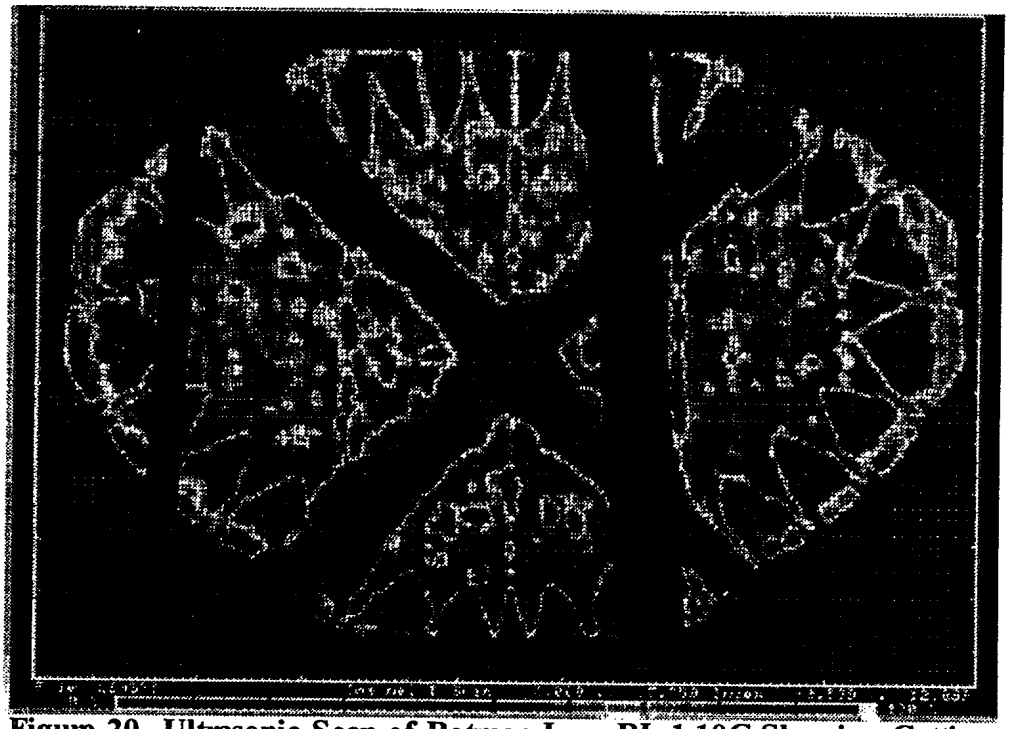

**Figure 20 Ultrasonic Scan of Rotman Lens RL 1.10C Showing Cutting Lines for Metallurgical Inspection**

In order to produce surfaces for examination which represent the actual interior of the lens, and not ones that are corrupted by the cutting and polishing processes, it was necessary to follow separation procedures that did not damage the lens. Trial cutting was conducted on the first cut to be made - the removal of the end of the lens for ultrasonic scan process validation. The process that was suggested by Spar Aerospace required that an initial cut, 0.5" wide and 0.2" deep, be made on both aluminum plates, followed by separation of the two pieces using a parallel-cut end mill. However, following the milling of the two 0.5" wide grooves, the resulting assembly did not have the stability to carry normal handling loads and, as a result, delaminated at one end. This process was thus abandoned. Instead, the lens was cut with a band saw along the desired line. Then about 0.001" of the exposed surface was removed in a milling machine, producing a fairly smooth surface. Specimens covering the areas of interest were removed for further processing. Surfaces were ground and polished to a mirror-like finish. Stepwise grinding was carried out on wet silicon carbide abrasive paper with grits 320, 400, 600, 800, and 1200. Running water was used as a lubricant throughout this stage. Between each grinding step the samples were ultrasonically cleaned in distilled water. Following grinding, the samples were then polished using 3 micron and then 1 micron diamond abrasive. Final polishing was carried out using a colloidal silica suspension. Ultrasonic cleaning in soapy water followed by rinsing with distilled water was performed between each of the polishing steps. After the completion of these processes, the specimens were examined under an optical microscope and micrographs were taken from areas of interest.

Examination of the specimens resulted in the verification of the C-scan results. A selection of the photos taken is shown in Figures 21 to 23. Each of these figures contains two photos of different magnifications. The upper and lower photos have magnifications of 40 and 160; in these photos, 8 mm on the photo corresponds to approximately 200 and 50 μm respectively.

Figure 21 is a cross-section of the splice area, and it clearly shows the inside edges of the external aluminum plates, the adhesive layers, the dielectric material, and the copper sheeting. The interfaces between the different layers can be seen, and appear to be clean and intact, especially in comparison to the other specimens. It can be seen that, in the area of the splice, the thickness of the adhesive layers joining the fingers of the splice within the top and bottom layers of the particular section shown is inconsistent. On the top layer the adhesive is about 12 μm thick, while on the bottom layer it is about 50 μm thick. Also, in the top layer, the space at the end of one of the fingers has been filled with adhesive. The lower photo shows the detail of the boundaries between the copper sheeting and the dielectric. The thickness of the adhesive is uniform, and the interface is without air gaps or disbond. It should be noted that the copper sheeting is actually approximately 40 μm thick, rather than 20 μm (corresponding to 0.0007" shown in Figure 4). The thickness of the dielectric and the adhesive is consistent with that shown in Figure 4.

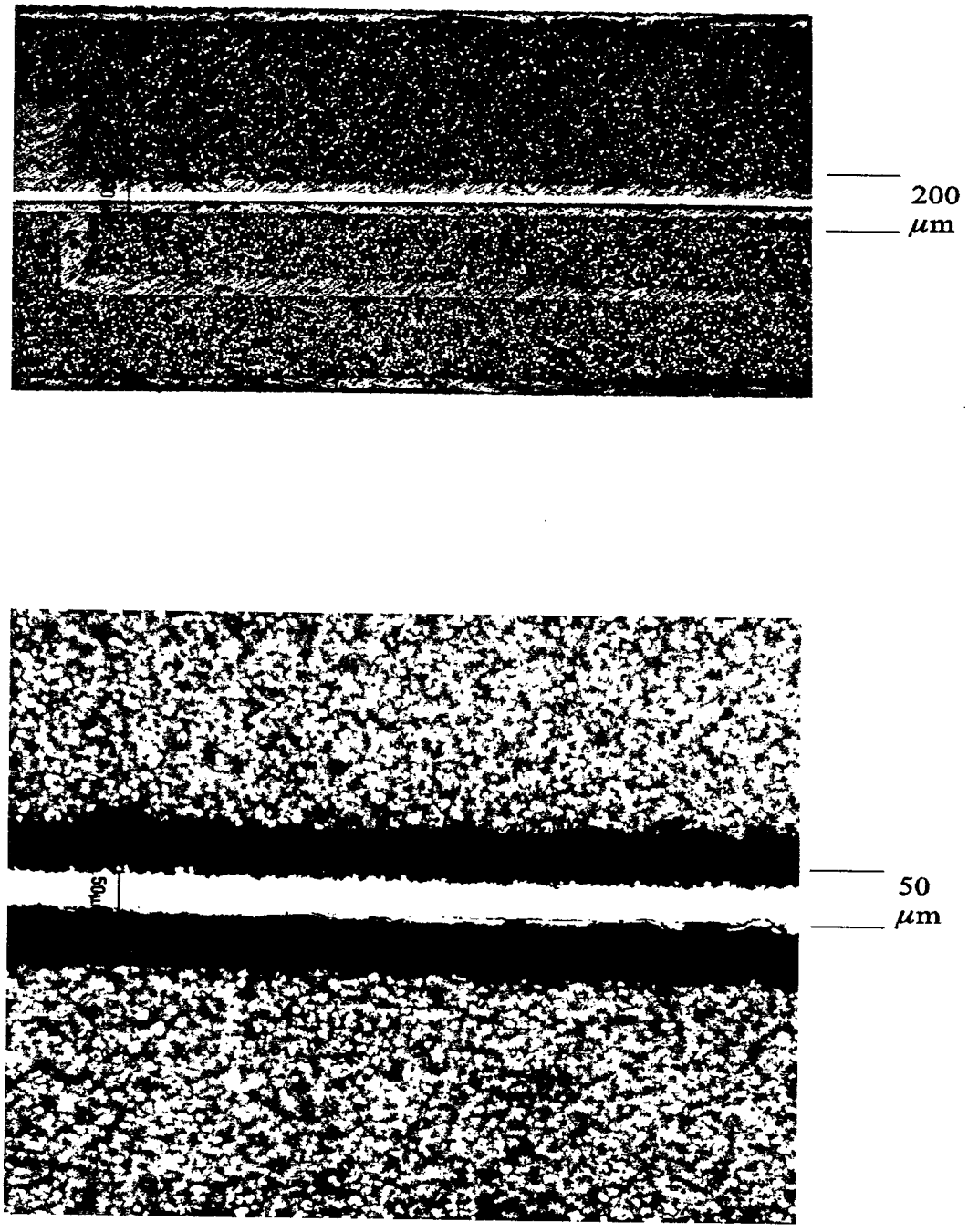


**Figure 21 Optical Micrographs of the Cross-Section of the Splice Area of Lens C**

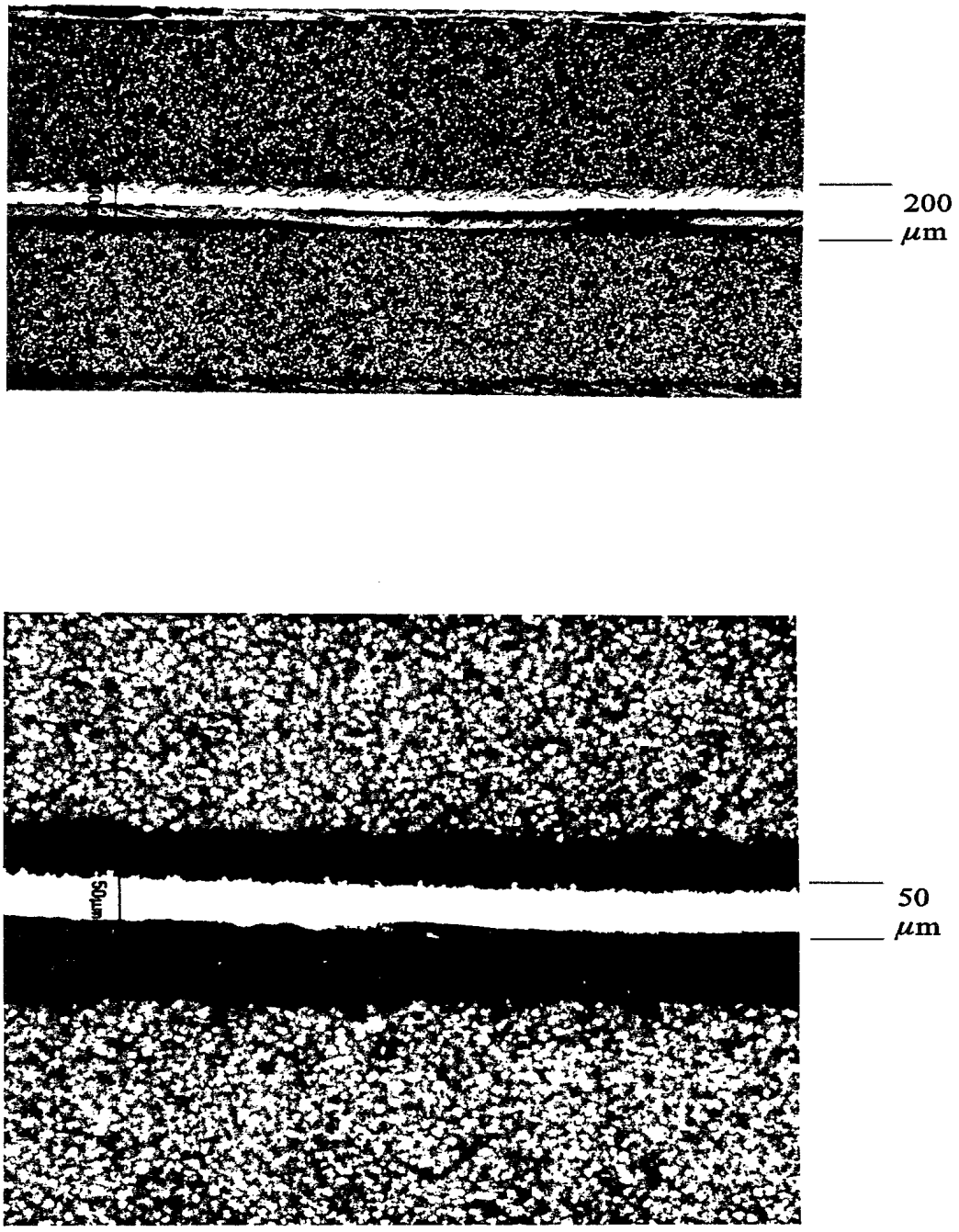


**Figure 22 Optical Micrographs of the Cross-Section of Lens C Showing Air Gaps Along the Dielectric/Adhesive Interface**

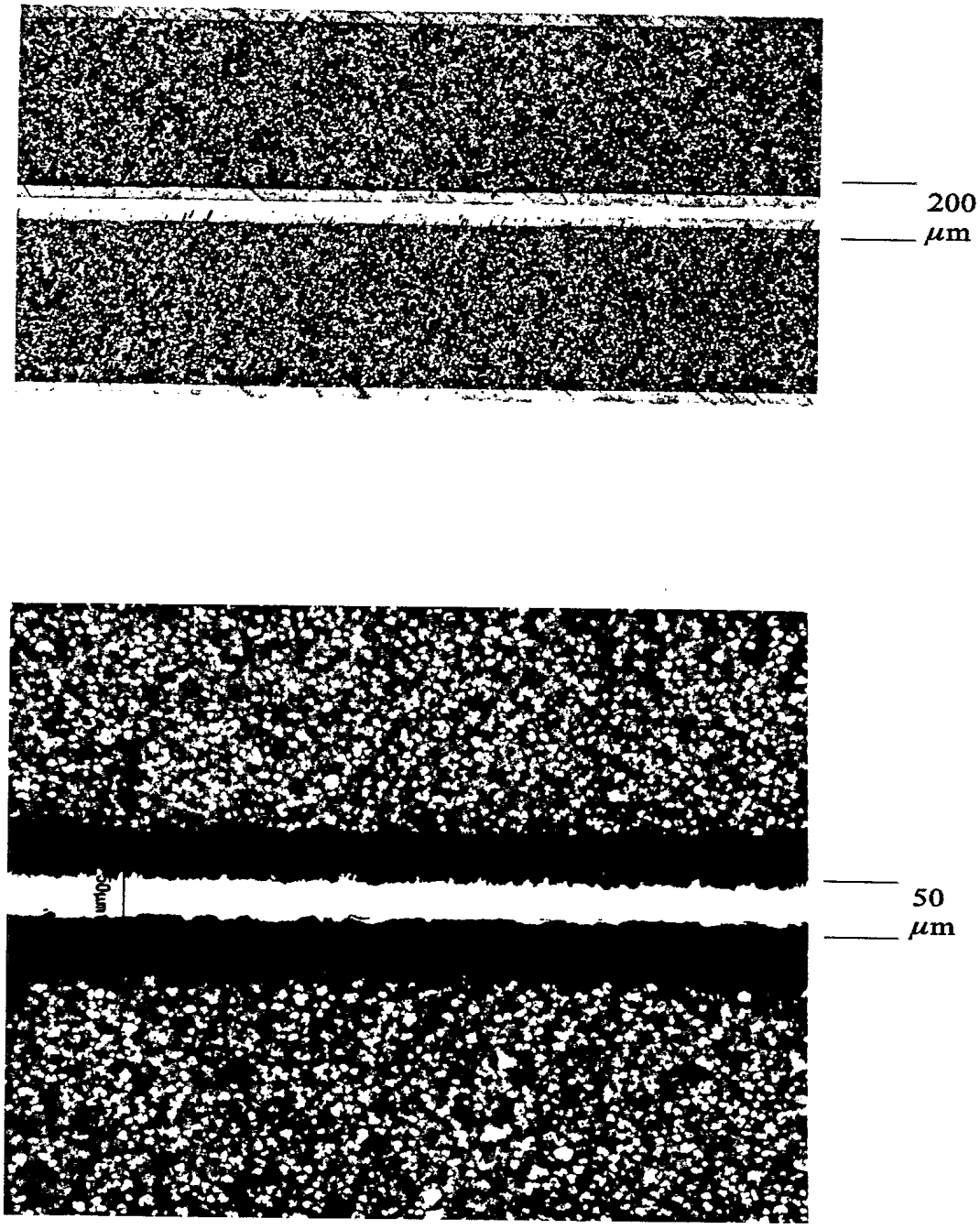


**Figure 23 Optical Micrographs of the Cross-Section of Lens C Showing Disbond Between the Dielectric Material and the Adhesive**

In Figure 22, air gaps can be seen along the interface between the dielectric material and the adhesive. For the most part, the boundary between the adhesive and the copper foil was without air gaps. The air gaps were as wide as 30 microns and their locations matched the locations of the flaws on the C-scans. It is unlikely that these gaps were generated during the cutting or polishing processes, since other regions of the same specimen were good, similar to those shown in Figure 21.

Micrographs were also taken from the entire polished surface of the second specimen. The photographs in Figure 23 were taken from a flawed region close to the centre of the lens. The micrographs indicated regions that suffered from a lack of a complete bond between the dielectric material and the adhesive layer. The location of the gap in the specimen corresponded to the location of the flaw indication on the C-scan image.

The microscopic inspection of one of the lenses has confirmed the presence of air gaps and disbond within the sectioned lens. Because of the similarities between the ultrasonic scans of that lens and those of the others, it is implied that the remaining lenses also contain similar defects. It is not known to what extent the presence of these flaws has degraded the RF performance of the lenses, and this was not able to be evaluated at this time.

# 3. ELECTRICAL EVALUATION

## 3.1 Introduction

In the design of a Rotman lens, one of the parameters that it is necessary to know is the effective dielectric constant of the dielectric material to be used in the internal region of the lens. The dielectric material determines the propagation properties for the electromagnetic waves within the lens, hence the overall design. Also, if the value used is incorrect, the impedance matching for the input and output ports will not be optimized. In this case, the throughput losses will be greater than expected because of mismatch losses. In addition, the energy within the lens will not be coupled out of the lens properly, resulting in reflected energy being dissipated at the dummy ports. Finally, if the dielectric constants of the top and bottom layers are different, the phase of the waves reaching the output connectors will not be the same, resulting in significant signal reflection at the impedance matching transformers.

A number of methods exist for measuring the effective permittivity of Microwave Integrated Circuit (MIC) materials. A selection of the techniques is described here. The first method involves the calculation of the permittivity from the measurement of the resonant frequencies of a simple parallel plate dielectric loaded resonator consisting of a rectangular substrate with its top and bottom surface metallization.[19] Another method, but similar, uses a cavity which has metallized sides as well as top and bottom.[20,21] Another publication[22] describes two different methods of measuring the permittivity which have errors of different sign; the accuracy is derived from the fact that when the values obtained are averaged, the mean is considered to be closer to the true value, the errors partially negating each other. Another reference[23] describes two methods, called the "Reflection Cancellation Method" and the "Line Balancing Method", for determining the permittivity specific to the length of the microstrip in question. Finally, a paper[24] describes a technique by which the dielectric constant of a complex structure can be determined by a combination of theoretical and experimental techniques. The complex structure consists of a metal strip mounted on a dielectric slab which is suspended at a distance over a ground plane. In this case, the guide wavelength is measured at a known frequency and the dielectric constant calculated from the measurement result. In all of the previous techniques, the measurements were made on a sample without destroying it, thus leaving it available for use. In the latter, a transmission line must be etched from the copper foil, thus eliminating the possibility of it being subsequently used.

After surveying various methods, it was decided to use a two transmission line method. In this method, the time or phase difference between two signals travelling over two transmission lines of different lengths that were manufactured on the same piece of substrate at the same time, is compared.[25] Calculations on the resulting data yield the dielectric constant. Providing both the lines have identical connectors and impedance transformers, their effects do not appear in the difference calculations, as

the only difference between them is the difference of the lengths. The method was originally proposed for use with microstrip transmission lines, where there is only dielectric on one side of the conductor. In this case it was used for stripline, which employs dielectric and ground plane on both sides of the conductor. The assumption in using this process in this way is that the dielectric constant of the material on both the top and bottom layers will be the same.

In the following discussion, the details of the measurement process are described, and equations derived for the determination of the dielectric constant based on either time or phase measurements. Results are then presented for transmission lines with different characteristic impedances. Conclusions are then drawn based on the results presented. In this way, an appreciation of the difficulties encountered in determining the dielectric constant of the dielectric material within the Rotman lenses is obtained.

## 3.2 Methodology for the Measurement of the Dielectric Constant

For the measurement of the effective dielectric constant of the material within the substrate, two transmission lines having the same impedance are etched onto a substrate, with one of them substantially longer than the other. This large difference in the length of the lines serves to increase the difference in transit time and rate of phase change with frequency between the lines. The setup for the measurement of the dielectric constant using two lines is illustrated in Figure 24 for 50 ohm transmission lines. Connections are made to the lines through end-launch RF connectors. In the case of transmission lines having an impedance that differs from 50 ohms, transitions are necessary so that the lines are matched to the source and load impedances to minimize reflections.

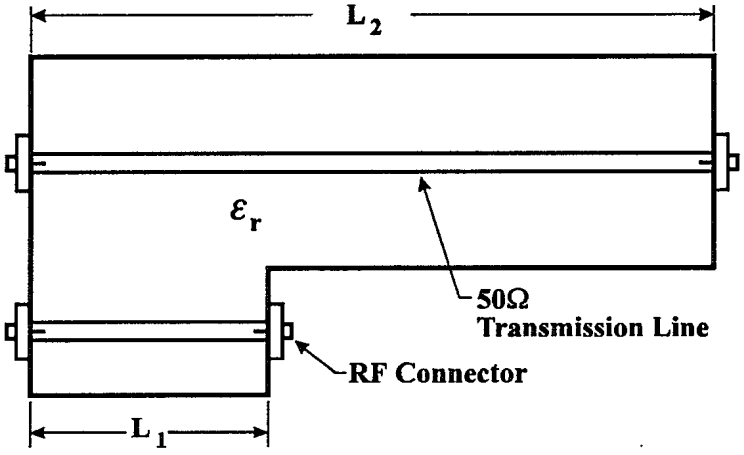


**Figure 24 Experimental Setup for the Two Line Method**

In the measurement process, the characteristics of the longer line, $L_2$ , are measured with respect to the shorter line, $L_1$ . For an arbitrary transmission line, at any frequency, the dielectric constant $\epsilon$ can be determined by

$$\epsilon = (\frac{\Delta l_e}{\Delta l_p})^2 = (\frac{c\ \Delta t}{\Delta l_p})^2 \qquad (2)$$

where $\Delta l_e$ is the measured electrical length of the line,
$\Delta l_p$ is the actual physical length of the line,
$c$ is the speed of light, and
$\Delta t$ is the measured transit time of the line.

When comparing two lines, the dielectric constant is determined by the measurement of the difference in the characteristics between two separate lines of different lengths. In this case, $\Delta l_e$ becomes the difference in the electrical lengths measured, $\Delta l_p$ is the actual difference in the physical lengths of the lines, and $\Delta t$ is the measured difference in transit time.

The dielectric constant can also be determined from phase difference measurements. The actual phase difference at a single frequency is difficult to determine, however the change in phase difference as a function of frequency is readily measured. Rearranging Equation (2), and also expressing the measured electrical length in terms of absolute phase measurement yields

$$\begin{aligned} \Delta l_e &= \sqrt{\epsilon}\ \Delta l_p \\ &= \frac{\Delta\theta}{360}\ \frac{c}{f} \end{aligned} \qquad (3)$$

where $\Delta\theta$ is the measured absolute phase difference in degrees, and
$f$ is the frequency.
Rearranging,

$$\Delta\theta = 360\ \frac{f}{c}\ \sqrt{\epsilon}\ \Delta l_p \qquad (4)$$

As mentioned, it is difficult to measure the absolute phase shift on the lines; however it is possible to measure the rate of change of the absolute phase shift as a function of frequency. Differentiating both sides of Equation (4),

$$\frac{d\ (\Delta\theta)}{df} = \frac{360}{c}\ \sqrt{\epsilon}\ \Delta l_p \qquad (5)$$

Solving for $\epsilon$ yields the expression

$$\epsilon = [\frac{c}{360\ \Delta l_p}\ \frac{d\ (\Delta\theta)}{df}]^2 \qquad (6)$$

As the frequency is changed, the phase changes, and it is this slope at the frequency of each measurement that is used in Equation (6). The results of each of these methods are discussed with the presentation of the data.

### 3.3 Dielectric Constant of the Stripline Substrate

At Spar Aerospace, a number of stripline circuits were fabricated to measure the relative permittivity of the dielectric material within the substrates. Transmission lines of 50, 30 and 1 ohm were fabricated and measurements made on them. The cross-section of the structures is the same as that used in the Rotman lenses, and is shown in Figure 4. These test lines are illustrated in Figures 25 and 26. For the 50 ohm lines, no impedance transformer was required, so the lines are of uniform width over the complete length. For the 30 ohm transmission line, a single stage transformer was used; for the 1 ohm line, a multiple stage transformer with a tapered section was used. This more complicated transformer was required because of the large change in impedance required. In those cases where a transformer was needed, an identical transformer was used at both ends of each of the two lines whose characteristics were to be compared.

Measurements were made using the Hewlett-Packard (HP) 8510C Vector Network Analyzer. Standard calibration and measurement procedures were used, and are not further described here.[26] At each frequency, 1000 readings were taken to reduce the effects of noise. This value was chosen by gradually increasing the number of points to be averaged until successive averaged readings were consistent. The magnitude of the attenuation, the phase shift and the delay of the long transmission line were all measured with respect to the shorter line. Formatted data files for all measurements and calibration exercises were written to computer disks so that they could be retrieved and analyzed at a later time. The data files were read in and formatted by a Basic program and rewritten in a format acceptable to the Excel program. All data calculation and plotting were done using Excel Version 4.0.

In Section 3.2, two different methods were described for the determination of the permittivity of the dielectric. One of these was based on the measurement of the difference in the delay of the two transmission lines and used Equation (2), and the other on the rate of change of the difference of the phase of the two lines as the frequency is changed, using Equation (6). Figures 27 and 28 are plots of the permittivity of the dielectric derived from the measurement of lines having a characteristic impedance of 50 ohms; the curve in Figure 27 is derived from the delay data, and that in Figure 28 on the phase data. It can be seen that the average

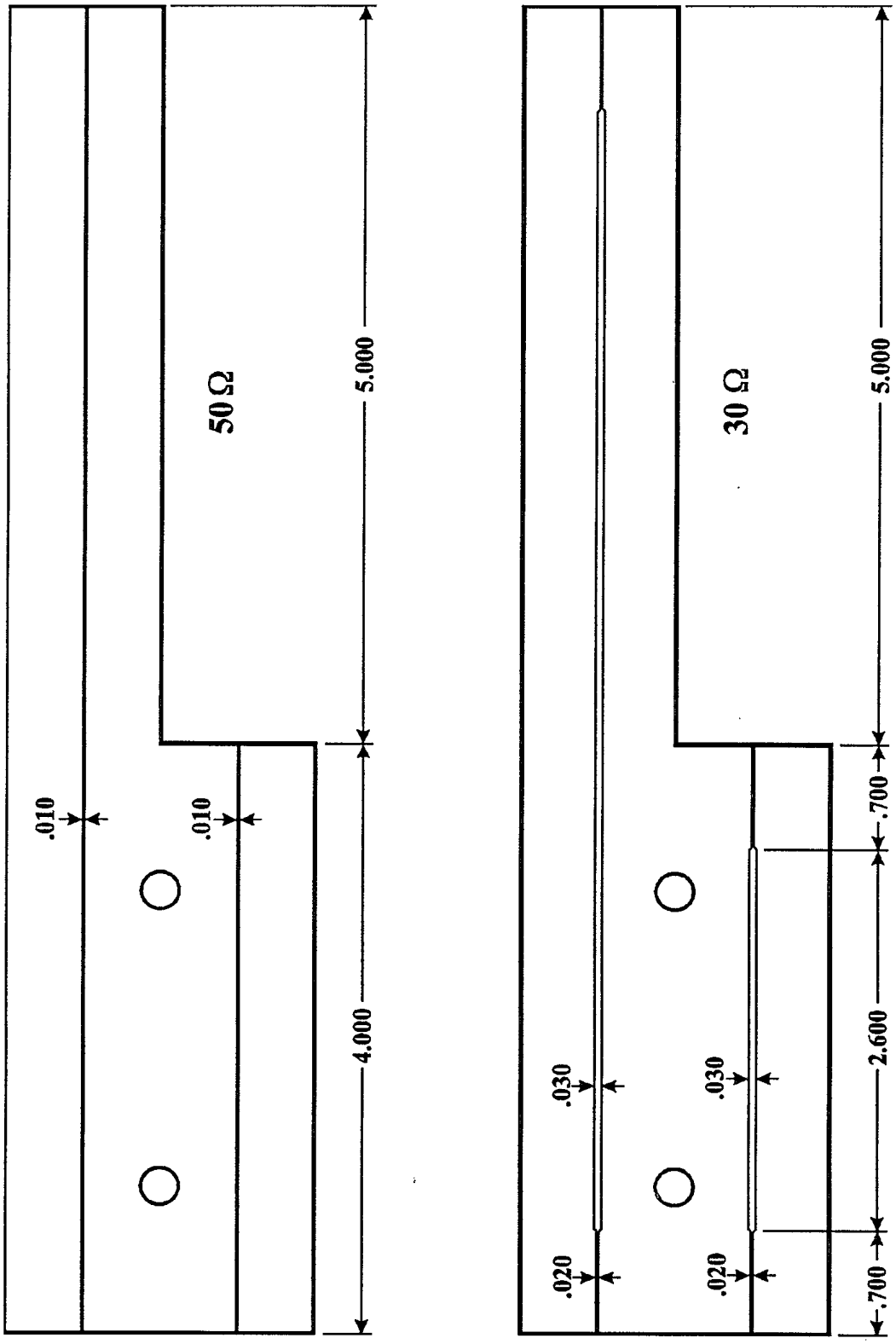


Figure 25. Dielectric Constant Measurement Using 30 and 50 Ohm Lines

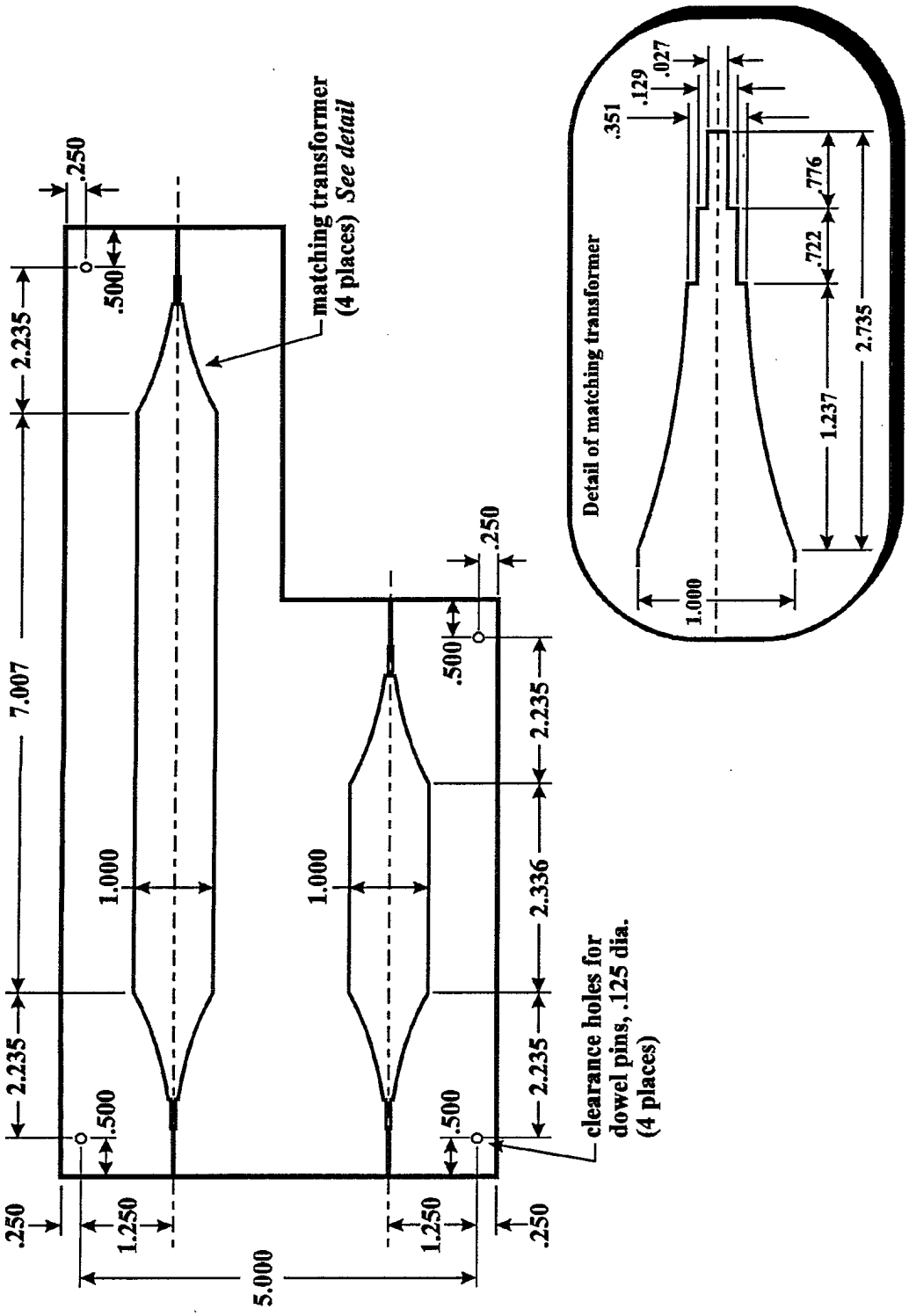


Figure 26. Dielectric Constant Measurement Using 1 Ohm Lines

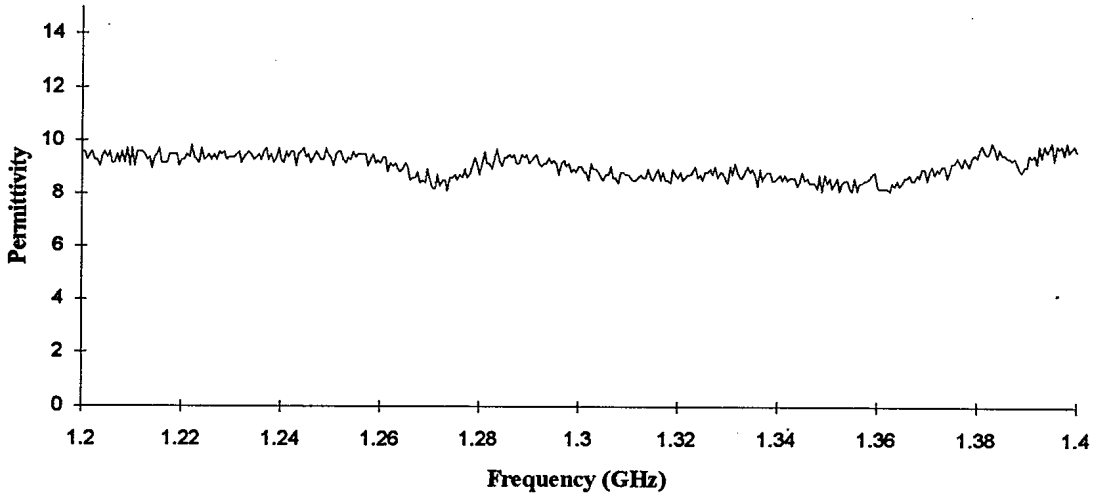


**Figure 27 Permittivity Based on Delay Data for 50 Ohm Lines**

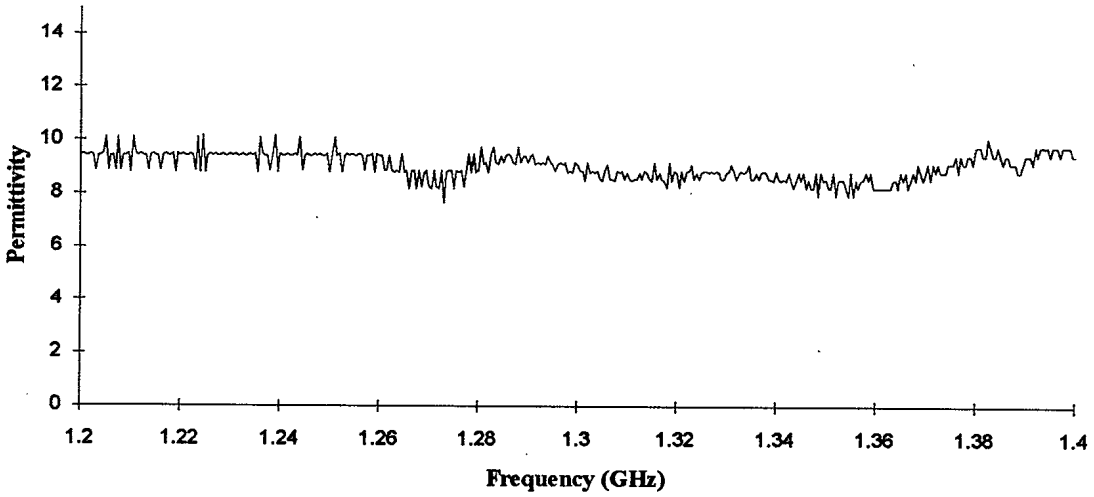


**Figure 28 Permittivity Based on Phase Data for 50 Ohm Lines**

variations as the frequency is varied are similar. In the curve derived from the phase data, however, the permittivity appears to have a tendency to take on discrete values; the reason for this is not understood, although it is expected that it might be a function of the measurement process, or be a result of some constraint of the measurement process. It was not investigated further. The permittivity values for the dielectric using 30 and 1 ohm lines were determined from the delay data. Figure 29 is a plot of the difference between the curves of Figures 27 and 28. The mean difference appears to be close to zero, indicating that the values track well, but it is important to notice that substantial variations between the two methodologies have occurred. Because 1000 readings were taken at each frequency, the differences were deemed not to be as a result of random time domain fluctuations in the readings. The differences up to 1.0 are significant, as the dielectric constant must be known much more accurately than that in order to obtain repeatable results after the fabrication of devices. In addition, in order to balance the Rotman lens, the dielectric constant must be within a few percent in order to prevent the signals in the upper and lower layers of the stripline structure from differing significantly in phase. For consistency, the permittivity obtained from the delay data is taken as being representative of the true values.

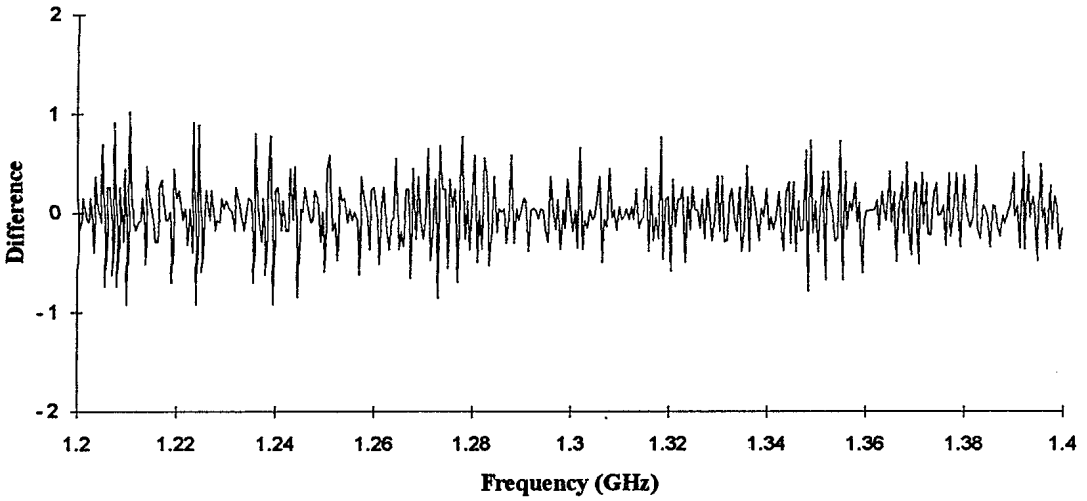


**Figure 29 Difference in Permittivity From Delay and Phase Data on 50 Ohm Lines**

The permittivity of the dielectric obtained through the analysis of the delay data from 30 and 1 ohm lines has also been obtained. It is shown in Figures 30 to 33. Structures were fabricated by Buckbee-Mears, St. Paul, MN, and CMR, Montreal, PQ. There is some consistency in the values obtained. For 50 ohm lines, the average permittivity is the highest, dropping somewhat for the 30 ohm lines, and reaching its lowest value for the 1 ohm lines. The two curves for 30 ohm lines show local maximum values near 1.3 GHz, and minimum values near 1.37 GHz. There seems to be a problem with the 1 ohm transmission line structure made by Buckbee-Mears. It

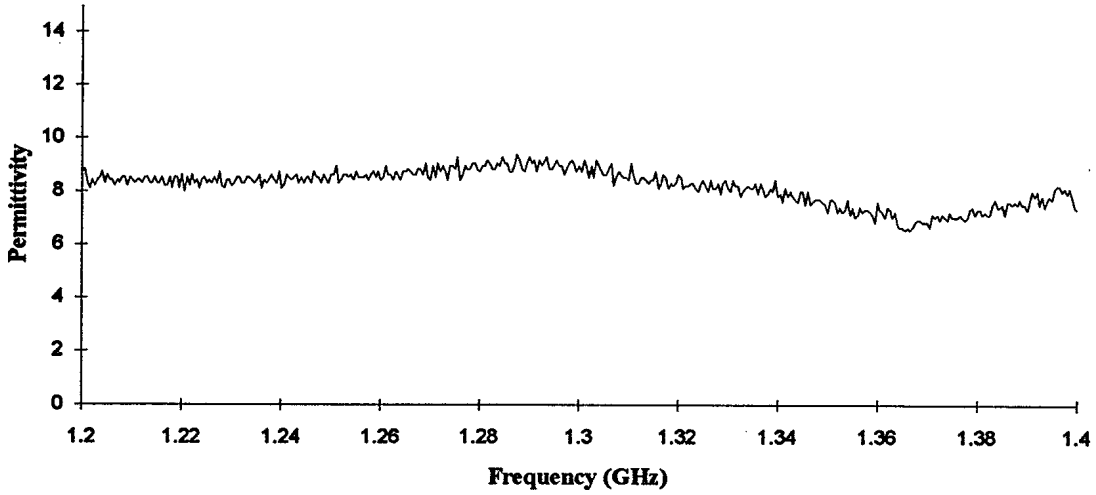


**Figure 30 Permittivity Based on Delay Data for 30 Ohm Lines Fabricated by Buckbee-Mears, St. Paul, MN**

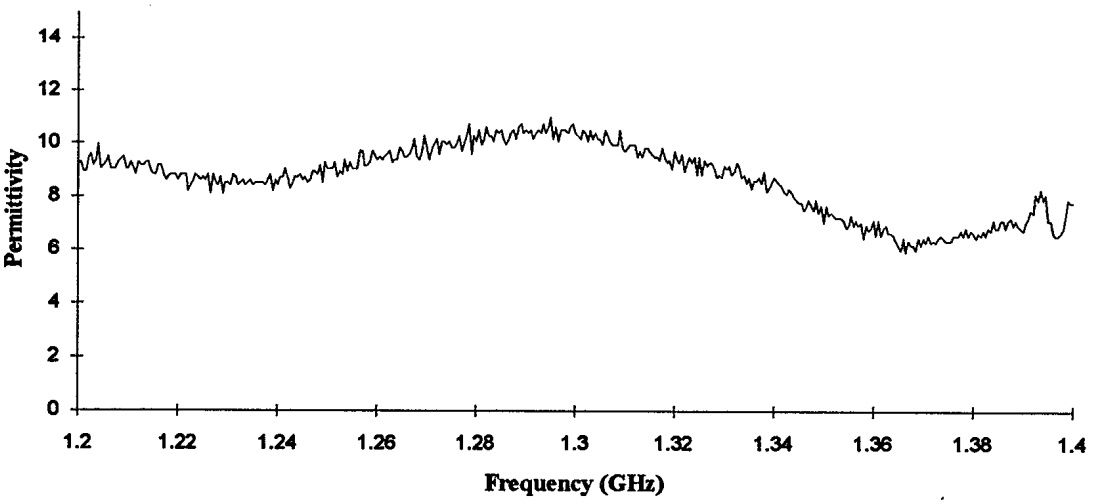


**Figure 31 Permittivity Based on Delay Data for 30 Ohm Lines Fabricated by CMR, Montreal, PQ**

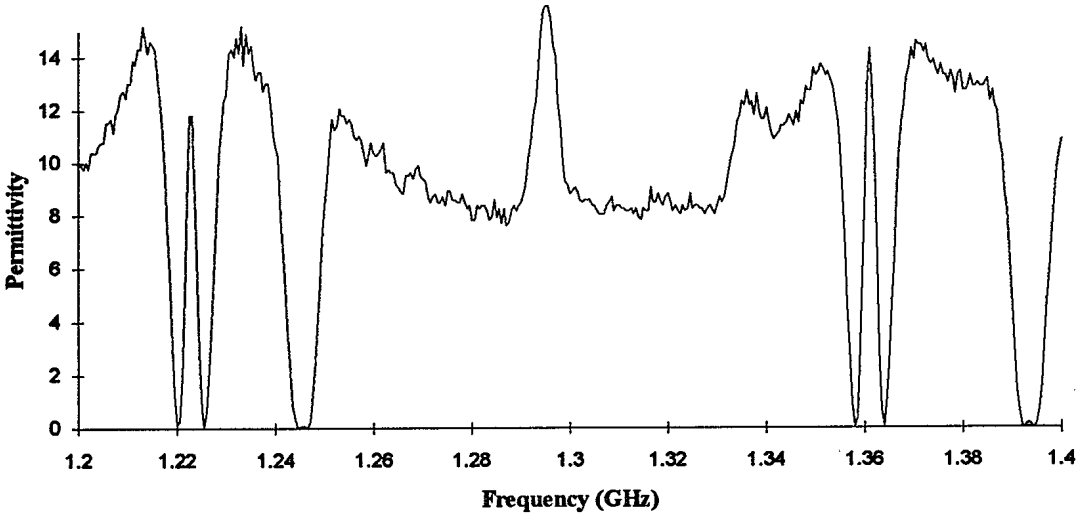


**Figure 32 Permittivity Based on Delay Data for 1 Ohm Lines Fabricated by Buckbee-Mears, St. Paul, MN**

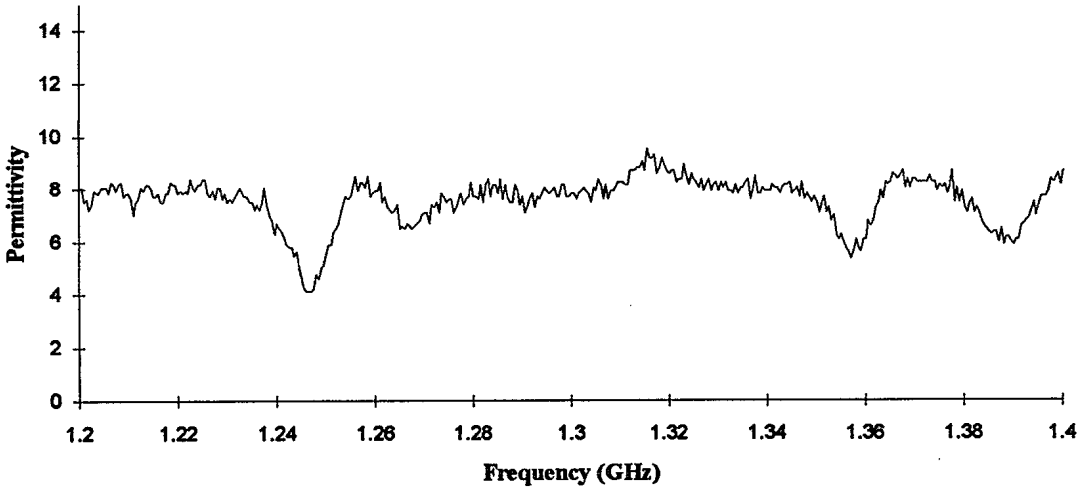


**Figure 33 Permittivity Based on Delay Data for 1 Ohm Lines Fabricated by CMR, Montreal, PQ**

has a number of deviations from the average. In an attempt to investigate these, the measurements were repeated with different cables and cables of different lengths. It is possibly caused by interactions at the connector, or inadequate bonding of the structure. Spar Aerospace also reported this problem in their contract report.[11]

In addition to measuring conventionally manufactured lines, measurements were also made on a structure that had been manufactured with one of the bonding layers adjacent to the copper foil omitted so that it could be disassembled. During measurement, this structure was held intact with moderate pressure with approximately 12 C-clamps. Some difficulties were experienced with this structure, as anomalies appeared in the curves that could not be traced to cabling or other physical phenomena. It was expected that these irregularities were a result of air voids within the structure because of the lack of even pressure from the clamps.

### 3.4 Discussion and Assessment

The results of the measurement of the differential delay between transmission lines of different lengths on the same structure have been presented. The actual value of the permittivity is difficult to determine from this set of measurements, as there is considerable fluctuation in the values. The reason for this fluctuation is unknown, and it is not known whether what was observed is the actual property of the dielectric or a result of some anomaly of the measurement process. Spar Aerospace reported values of permittivity for experiments that involved the measurement of structures that had no adhesive, and others bonded with a variety of adhesives.[11] A range of values were reported, and depended on the impedance of the line chosen, and whether or not the different layers of the structure had been bonded with an adhesive. Spar also reported difficulties with the low impedance structure fabricated by Buckbee-Mears; this is in agreement with our observations.

In order to confirm the true nature of the dielectric material in the structure, another method of determining its permittivity could be investigated. Other methods have been identified in this report, and consist of measurements made on cavities, and similar structures. The permittivity can also be measured on bulk materials.[27] Many of these techniques are destructive, or require that the material be measured in a configuration unlike that in which it will be used. (Remember that the effective dielectric constant measured was a function of the impedance of the lines, and thus their width.) This exercise, conducted to determine the permittivity of the dielectric, has not been able to reach conclusive results, except to indicate that the determination of the properties of the bonded dielectric is not a trivial process.

The conclusion from the Spar Aerospace investigations is that the problems arose when a higher dielectric constant substrate material ( $\epsilon_r \approx 10$ ) was bonded with a lower dielectric adhesive film ( $2.5 \leq \epsilon_r \leq 3.0$ ). The potentially uneven distribution of the low dielectric material in the presence of high dielectric material tends to generate parallel plate waveguide modes which are trapped modes. The wider the lines, the greater the generation of these modes. The connectors attached to the edges of the substrate material were unable to couple this energy out of he substrate. This was manifested in reduced output power from the port, and higher loss of the device.[14] These conclusions could not be confirmed in this study, although they are not disputed. Some unevenness of the low dielectric adhesive material was observed in the photomicrographs.

# 4. CONCLUSIONS AND RECOMMENDATIONS

This report has described an assessment of Rotman lenses designed and manufactured in support of the Space-Based Radar R&D Project at DREO. In a development program, four small Rotman lenses, and then one large one, were designed, manufactured and tested. Shortcomings in most aspects of the RF performance have prompted further investigations. Without funds for the fabrication of additional devices, different measurements were devised which might lead to more insight into those that existed. Thus, it was decided to investigate physical mechanisms that could have impacted on the performance. For this reason, ultrasonic scanning and x-ray technologies were employed. Scans of the Rotman lenses revealed irregularities, possibly air voids, within some of the lenses, particularly along the dielectric splices between the different dielectric sheets. A scan of the large Rotman lens revealed a relatively clean implementation with few abnormalities. This might possibly indicate that the poor RF performance is not only due to the presence of air voids but possibly other physical anomalies.

In order to validate the results of the ultrasonic scans, one of the Rotman lenses was sectioned and metallurgically examined under a microscope. This revealed the presence of air voids at locations identified in the ultrasonic scans, confirming the results of the ultrasonic scanning process.

Finally, some of the measurements performed to determine the permittivity of the dielectric within the stripline material were repeated. This gave an indication of the difficulty in measuring this property. The permittivity was found to be a function of the impedance of the lines in the structure, and because of fluctuations, was difficult to determine.

The conclusions that can be drawn from the assessment of microwave stripline circuits by ultrasonic techniques are:

1. Ultrasonic testing can successfully identify the presence of surface texture and other internal surface features on the ground planes of a stripline circuit.

2. Ultrasonic testing can successfully identify the presence of voids between the layers of a stripline circuit; however, it cannot determine which layers they are between.

3. Ultrasonic testing can successfully identify the presence of splices in the dielectric material within a stripline circuit.

4. The presence of voids of the type found can be easily detected by ultrasonic sensors operating at all the frequencies of choice, 5, 10, 15, and 25 MHz.

The conclusions that can be drawn from the measurements of the Rotman lenses are:

5. Voids, possibly containing air, were found between the impedance matching transformers in almost all of the lenses tested.

6. Voids, possibly containing air, were found trapped under milling overlap areas on two of the lenses tested.

7. Voids, possibly containing air, were found trapped within the central area of the lens containing the dielectric splice.

8. No conclusions could be made regarding the effect of the presence of the air gaps found, and uneven thicknesses of adhesive, within the lenses, on their RF performance.

The conclusions that can be drawn from the measurement of the permittivity of the dielectric are:

9. The permittivity that was measured using the two line method is a function of the impedance (width) of the lines.

10. In some cases, the permittivity was a complex function of frequency.

11. The results of the measurement of the permittivity using the two methods discussed were similar in average values as a function of frequency, however the instantaneous values as a function of frequency did not agree so well.

## 5.0 References


1. Rotman, W., Turner, R.F., "Wide-Angle Microwave Lens for Line Source Applications", IEEE Transactions on Antennas and Propagation, November 1963, pp. 623-632.

2. Southall, Hugh L., McGrath, Daniel T., "An Experimental Completely Overlapped Subarray Antenna", IEEE Transactions on Antennas and Propagation, Vol. 34, No. 4, April 1986, pp. 465-474.

3. "Airborne Phased Array Antennas Will Enhance Jammer Effectiveness", Aviation Week and Space Technology, 14 April 1986, pp. 95-101.

4. Monser, George J., "Advances in Lens-Fed Multibeam Technology", Proceedings of the 1991 Antenna Applications Symposium, 25-27 September 1991, Royal Allerton Park, University of Illinois.

5. Chan, K. K., Tam, W., "Field Analysis of Planar Bootlace Lens Feeds", International Conference on Radar, April 1989, Paris, France, Vol. 1, pp. 273-278.

6. Chan, K. K., Wallace, W. B., Blasing, R. R. "Design of a Broadband and Wide Scan Angle Rotman Lens", IEEE AP-S International Symposium, May 1990, Dallas, Texas, Vol. 2, pp. 988-991.

7. Chan, K. K., Faubert, D., Martin, R. "Multiple Beam Antenna Feed Networks", Journees internationales de Nice sur les antennes, JINA 90, November 1990, Nice, France, pp. 333-336.

8. Practical Phased Array Antenna Systems, Brookner, Eli, Artech House, Norwood, MA, 1991.

9. "Rotman Lens Development for Space-Based Radar, Final Documentation, Volume I: Summary Report", Report RML-009-89-133, Spar Aerospace, Ste-Anne-de-Bellevue, Quebec, Canada, December 1989.

10. "Rotman Lens Development for Space-Based Radar, Final Documentation, Volume II: Specifications and Test Plans", Report RML-009-90-002, Spar Aerospace, Ste-Anne-de-Bellevue, Quebec, Canada, December 1989.

11. "Rotman Lens Development for Space-Based Radar, Final Documentation, Volume IIIA: Rotman Lens Design, Implementation, and Test Report", Report RML-009-89-116, Spar Aerospace, Ste-Anne-de-Bellevue, Quebec, Canada, December 1989.

12. "Rotman Lens Development for Space-Based Radar, Final Documentation, Volume IIIB: Radiating Array Design, Implementation, and Test Report", Report RML-009-89-114, Spar Aerospace, Ste-Anne-de-Bellevue, Quebec, Canada, December 1989.

13. "Rotman Lens Development for Space-Based Radar, Final Documentation, Volume IIIC: Receive Network Design, Implementation, and Test Report", Report RML-009-89-115, Spar Aerospace, Ste-Anne-de-Bellevue, Quebec, Canada, December 1989.

14. "Rotman Lens Development for Space-Based Radar, Phase II, Investigation of the Causes for the Non-Performance of the Lens, Final Report", Report RML-009-90-085, Spar Aerospace, Ste-Anne-de-Bellevue, Quebec, Canada, November 1990 .

15. Metals Handbook, 8th ed., American Society for Metals, Metals Park, Ohio, 1976, Chapter 11, pp. 161-198.

16. Ultrasonic Testing of Materials, Third ed., Krautkramer, J., Krautkramer, H., Springer-Verlag, New York, 1983.

17. Fahr, A., Chapman, C.E., "Inspection of Rotman Lenses", NRC Structures and Materials Laboratory, Report No. ST-689, 24 November 93.

18. Private Communication, S. Rao, Spar Aerospace Ltd., Ste. Anne de Bellevue, P.Q.

19. Napoli, L. S., Hughes, J. J., "A Simple Technique for the Accurate Determination of the Microwave Dielectric Constant for Microwave Integrated Circuit Substrates", IEEE Transactions on Microwave Theory and Techniques, July 1971, pp. 664-665.

20. Howell, John Q., "A Quick Accurate Method to Measure the Dielectric Constant of Microwave Integrated-Circuit Substrates", IEEE Transactions on Microwave Theory and Techniques, March 1973, pp. 142-143.

21. Ladbrooke, P. H., Potok, M. H. N., England, E. H., "Comments on "A Quick Accurate Method to Measure the Dielectric Constant of Microwave Integrated-Circuit Substrates"", IEEE Transactions on Microwave Theory and Techniques, August 1973, pp. 570-571.

22. Ladbrooke, P. H., Potok, M. H. N., England, E. H. "Coupling Errors in Cavity-Resonance Measurements on MIC Dielectrics", IEEE Transactions on Microwave Theory and Techniques, August 1973, pp. 560-562.

23. Pannell, R. M., Jervis, B. W., "Two Simple Methods for the Measurement of the Dielectric Permittivity of Low-Loss Microstrip Substrates", IEEE Transactions on Microwave Theory and Techniques, MTT-29, No. 4, April 1981, pp. 383-386.

24. Hubbell, S., Angelakos, D. J., "A Technique for Measuring the Effective Dielectric Constant of a Microstrip Line", IEEE Transactions on Microwave Theory and Techniques MTT-31, No. 8, August 1983, pp. 687-688.

25. Das, Nirod K., Voda, Susanne M., and Pozar, David M., "Two Methods for the Measurement of Substrate Dielectric Constant", IEEE Transactions on Microwave Theory and Techniques MTT-35, No. 7, July 1987, pp. 636-642.

26. "HP 8510B Introductory Users Guide", Hewlett Packard Product Note 8510-10, July 1, 1988.

27. "Basics of Measuring the Dielectric Properties of Materials", Hewlett Packard Product Note 1217-1, March 1992.

UNCLASSIFIED

SECURITY CLASSIFICATION OF FORM
(highest classification of Title, Abstract, Keywords)

# DOCUMENT CONTROL DATA

(Security classification of title, body of abstract and indexing annotation must be entered when the overall document is classified)

**1. ORIGINATOR** (the name and address of the organization preparing the document. Organizations for whom the document was prepared, e.g. Establishment sponsoring a contractor's report, or tasking agency, are entered in section 8.)

Defence Research Establishment Ottawa
Ottawa, Ontario
K1A 0Z4

**2. SECURITY CLASSIFICATION** (overall security classification of the document including special warning terms if applicable)

UNCLASSIFIED

**3. TITLE** (the complete document title as indicated on the title page. Its classification should be indicated by the appropriate abbreviation (S,C or U) in parentheses after the title.)

Evaluation of Rotman Lenses for Space-Based Radar (U)

**4. AUTHORS** (Last name, first name, middle initial)

Moffat, John W.

**5. DATE OF PUBLICATION** (month and year of publication of document)

December 1995

**6a. NO. OF PAGES** (total containing information. Include Annexes, Appendices, etc.)

63

**6b. NO. OF REFS** (total cited in document)

27

**7. DESCRIPTIVE NOTES** (the category of the document, e.g. technical report, technical note or memorandum. If appropriate, enter the type of report, e.g. interim, progress, summary, annual or final. Give the inclusive dates when a specific reporting period is covered.

DREO Report

**8. SPONSORING ACTIVITY** (the name of the department project office or laboratory sponsoring the research and development. Include the address.

Space-Based Radar R&D, Defence Research Establishment Ottawa
Ottawa, Ontario, K1A 0Z4

**9a. PROJECT OR GRANT NO.** (if appropriate, the applicable research and development project or grant number under which the document was written. Please specify whether project or grant)

041BD

**9b. CONTRACT NO.** (if appropriate, the applicable number under which the document was written)

**10a. ORIGINATOR'S DOCUMENT NUMBER** (the official document number by which the document is identified by the originating activity. This number must be unique to this document.)

DREO REPORT 1271

**10b. OTHER DOCUMENT NOS.** (Any other numbers which may be assigned this document either by the originator or by the sponsor)

**11. DOCUMENT AVAILABILITY** (any limitations on further dissemination of the document, other than those imposed by security classification)

(X) Unlimited distribution
( ) Distribution limited to defence departments and defence contractors; further distribution only as approved
( ) Distribution limited to defence departments and Canadian defence contractors; further distribution only as approved
( ) Distribution limited to government departments and agencies; further distribution only as approved
( ) Distribution limited to defence departments; further distribution only as approved
( ) Other (please specify):

**12. DOCUMENT ANNOUNCEMENT** (any limitation to the bibliographic announcement of this document. This will normally correspond to the Document Availability (11). however, where further distribution (beyond the audience specified in 11) is possible, a wider announcement audience may be selected.)

Unlimited Announcement

UNCLASSIFIED

SECURITY CLASSIFICATION OF FORM

13. **ABSTRACT** (a brief and factual summary of the document. It may also appear elsewhere in the body of the document itself. It is highly desirable that the abstract of classified documents be unclassified. Each paragraph of the abstract shall begin with an indication of the security classification of the information in the paragraph (unless the document itself is unclassified) represented as (S), (C), or (U). It is not necessary to include here abstracts in both official languages unless the text is bilingual).

The Space-Based Radar (SBR) R&D Project at DREO has been investigating the feasibility of the application of a number of different technologies to space-based wide area surveillance using microwave radar. One of the technologies investigated was the Rotman lens implementation of a Fourier transform beam forming network. A number of Rotman lenses were designed and manufactured in stripline microwave structure under a development contract. The expected performance was not achieved. A study was intitiated to investigate possible causes of this performance deficiency.

This study was divided into two main thrusts. First the lenses were assessed physically using ultrasonic and X-ray technologies, with a confirmation of the results by the sectioning and subsequent microscopic examination of one of the lenses. Following that, some simple stripline structures were measured in a microwave lab in order to gain in order to gain an understanding of the difficulties of measuring the permittivity of the dielectric material within the structure. This report describes the experiments performed and the results obtained.

14. **KEYWORDS, DESCRIPTORS or IDENTIFIERS** (technically meaningful terms or short phrases that characterize a document and could be helpful in cataloguing the document. They should be selected so that no security classification is required. Identifiers, such as equipment model designation, trade name, military project code name, geographic location may also be included. If possible keywords should be selected from a published thesaurus. e.g. Thesaurus of Engineering and Scientific Terms (TEST) and that thesaurus-identified. If it is not possible to select indexing terms which are Unclassified, the classification of each should be indicated as with the title.)

Beam Forming Network
Dielectric Constant
Dielectrics
Fourier Transform BFN
Metallurgy
Microwave Radar
Permittivity
Rotman Lens
Space-Based Radar
Stripline
Ultrasonics
X-Rays

155548